Marine Micropaleontology 153 (2019) 101783

Contents lists available at ScienceDirect

Marine Micropaleontology

journal homepage: www.elsevier.com/locate/marmicro

Research paper

Evaluation and application of foraminiferal element/calcium ratios: Assessing riverine fluxes and environmental conditions during sapropel S1 in the Southeastern Mediterranean

M. Mojtahid[a,*], R. Hennekam[b,c], L. De Nooijer[c], G.-J. Reichart[b,c], F. Jorissen[a], W. Boer[c], S. Le Houedec[a], G.J. De Lange[b]

[a] LPG-BIAF UMR-CNRS 6112, UNIV Angers, UNIV Nantes, CNRS, UFR Sciences, 2 bd Lavoisier 49045, Angers Cedex 01, France
[b] Department of Earth Sciences-Geochemistry, Faculty of Geosciences, Utrecht University, P.O. Box 80.021, 3508 TA, Utrecht, The Netherlands
[c] Department of Ocean Systems, NIOZ Royal Netherlands Institute for Sea Research, Department of Ocean Systems, Utrecht University, P.O. Box 59, 1790 AB Den Burg, Texel, The Netherlands

ARTICLE INFO

Keywords:
Sapropel S1
Levantine basin
Productivity
Oxygenation
Salinity
Stable isotopes
Mg/Ca
Ba/Ca
Mn/Ca
Na/Ca

ABSTRACT

Paleostudies often rely on foraminiferal calcite chemistry, which reflect past sea water condition through so-called proxy relationships. One way to evaluate robustness of these proxy relationships is to test them in well-studied and during well-constrained climate transitions. The southeastern (SE) Mediterranean is a perfect natural laboratory with a large range of past environmental conditions. These range from low productivity well-ventilated waters like they are at present, to poorly ventilated, high productivity conditions during sapropels. We here explore the reliability of recently developed foraminiferal-based proxies (Ba/Ca, Mn/Ca, Na/Ca) as tracers for changes in productivity, oxygenation and salinity during the most recent sapropel S1. We use laser ablation ICP-MS analyses of the planktonic *G. ruber* and six benthic species (*B. alata*, *G. affinis*, *G. altiformis*, *G. orbicularis*, *H. boueana*, *U. peregrina*). Our results show that planktonic Ba/Ca is a reliable tracer for Ba^{2+}-enriched Nile outflow, where benthic Ba/Ca traces enhanced paleo(export) productivity relatively well. The interpretation of Mn/Ca data is less straightforward, and the low values may suggest a lower precipitation of Mn-oxides under prevailing hypoxia. The decrease in planktonic and benthic Na/Ca is coherent with excess Nile runoff lowering salinities in the < 500m water column. However, when applying the existing calibrations, unrealistic salinity values are found, highlighting potential secondary controls on Na-incorporation. Benthic Ba/Ca time series analyses highlight a multicentennial variability in paleo(export) productivity, consistently with redox proxies. We conclude that benthic Ba/Ca records the close coupling between Ba cycling, export productivity, and redox conditions during S1 in the SE Mediterranean.

1. Introduction

Element concentrations and stable isotope ratios in the tests of foraminifera can be used to reconstruct past environments and climates (e.g. Lea, 1999; Lynch-Stieglitz, 2003; Katz et al., 2010; Lea, 2014). Application of foraminiferal calcite chemistry depends on calibrations between incorporated elements/fractionated isotopes and one or more environmental parameters (e.g. Nehrke et al., 2013; Mewes et al., 2015; Langer et al., 2016). For instance, foraminiferal $\delta^{18}O$, which is one of the most widely applied proxies, depends on the temperature and the $\delta^{18}O$ of the seawater, which in turn is defined as a function of both global ice volume and local salinity affected by evaporation and precipitation (e.g. Shackleton, 1974; Rohling and Cooke, 2003). The use of foraminiferal trace/minor element incorporation (El/Ca) as an environmental proxy started with Hester and Boyle (1982) showing that Cadmium (Cd) is incorporated into benthic foraminiferal tests proportionally to the Cd concentration of ambient seawater. This allowed thereby applying Cd/Ca as a proxy for deep-ocean circulation and nutrient chemistry (e.g. Marchitto and Broecker, 2006; Lynch-Stieglitz et al., 2007). Since then, calibrations were developed for a suite of elements using culture experiments, plankton tows, sediment traps and core-top studies (e.g. Boyle, 1995; Rosenthal et al., 1997; Lea, 1999; Lear et al., 2002; Elderfield et al., 2006; Rosenthal et al., 2011; Schmittner et al., 2017). Ideally, these proxies are influenced by a single environmental variable, which in reality is rarely the case (e.g. Nürnberg et al., 1996; Elderfield et al., 2006). Despite the

* Corresponding author.
E-mail address: meryem.mojtahid@univ-angers.fr (M. Mojtahid).

https://doi.org/10.1016/j.marmicro.2019.101783
Received 18 June 2019; Received in revised form 16 September 2019; Accepted 30 September 2019
Available online 25 October 2019

acknowledged limitations and uncertainties, the Mg/Ca ratio of foraminiferal calcite is a widely applied empirical proxy for ocean temperature (e.g. Elderfield et al., 2002; Lea et al., 2000; Nürnberg et al., 2000; de Garidel-Thoron et al., 2005; Bohaty et al., 2012; Branson et al., 2013; Gray et al., 2018; Gray and Evans, 2019). However, in addition to species-specific differences that can be overcome by robust calibration studies (e.g. Nürnberg et al., 1996; Anand et al., 2003; Elderfield et al., 2006), evidence suggests that foraminiferal Mg incorporation is affected by other environmental parameters such as salinity (e.g. Lea et al., 1999; Dueñas et al., 2011; Honisch et al., 2013), carbonate ion concentration (e.g. Elderfield et al., 2006; Rosenthal et al., 2006) and Mg/Ca of the seawater (e.g. Segev and Erez, 2006). More recently Ba/Ca, Mn/Ca, and Na/Ca ratios in foraminiferal calcite were proposed as proxies for productivity, oxygenation and salinity, respectively:

Incorporation of Barium in foraminiferal calcite is proportional to seawater Ba concentrations (e.g. Lea and Boyle, 1989, 1990; Lea and Spero, 1992; de Nooijer et al., 2017). In surface waters adjacent to the continent, seawater [Ba^{2+}] can reflect salinity due to the relatively high Ba/Ca of rivers or meltwater input (Guay and Kenison Falkner, 1997, 1998) and thus Ba/Ca in planktonic foraminifera can be used to reconstruct past salinities in these environments (e.g. Weldeab et al., 2007, 2014; Bahr et al., 2013). Because biogenic barite ($BaSO_4$) forms as microcrystals in decaying organic debris, $BaSO_4$ burial fluxes are strongly linked to surface marine productivity (e.g. Dymond et al., 1992; Dymond and Collier, 1996; Paytan and Griffith, 2007; Liguori et al., 2016). After burial at the seafloor, $BaSO_4$ partially dissolves in undersaturated bottom waters and as such, Ba/Ca in benthic foraminifera can be used as a proxy for bottom-water Ba concentrations and implicitly, paleoproductivity (e.g. Ní Fhlaithearta et al., 2010).

Manganese is a redox-sensitive element, mainly present as Mn^{2+} in sea water but precipitating as Mn oxyhydroxides under oxygenated conditions. Under low-oxygen conditions in the sediment and/or in bottom waters, Mn oxyhydroxides are reduced and Mn^{2+} is released (see review in Lea, 1999). Thus, ideally, when benthic foraminifera precipitate in these conditions, more Mn will be incorporated into their calcite tests and high Mn/Ca may therefore be used as a proxy for low-oxygen conditions (e.g. Reichart et al., 2003; Ní Fhlaithearta et al., 2010; Groeneveld and Filipsson, 2013; McKay et al., 2015; Koho et al., 2017; Barras et al., 2018).

The link between Na content of biogenic carbonates and salinity was first proposed by Rucker and Valentine (1961) for the Atlantic oyster *Crassostrea virginica*, and confirmed later by Gordon et al. (1970) in fossil barnacle shells. More recently, several studies report a positive correlation between the Na/Ca of foraminiferal tests and Na which resulted in a newly proposed paleosalinity proxy (e.g. Wit et al., 2013; Allen et al., 2016; Mezger et al., 2016, 2018, 2019). This correlation was explained by a relative increase in activity of free [Na^{+}] compared to [Ca^{2+}] activity with increasing salinity (Wit et al., 2013).

The eastern Mediterranean is a perfect natural laboratory to validate the reliability of these proxies due to the succession of sapropel deposits (e.g. De Lange et al., 2008). Deposition of these organic-rich layers is caused by: (i) freshwater flooding leading to stagnant bottom waters with reducing conditions, and (ii) high primary production (e.g. Rossignol-Strick et al., 1982; Rohling, 1994; van der Meer et al., 2007), both of which allow validating (novel) proxies. The driving force for these events is strongly associated to North African monsoon intensity fueling rivers such as the Nile, affecting the Mediterranean surface and deep water circulation (e.g. De Lange et al., 2008; Rohling et al., 2015). The present study focuses on the most recent sapropel (S1; ~10 to 6 cal ka BP) from a marine sediment core PS009PC located in the southeastern (SE) Levantine Basin (Fig. 1.). Core PS009PC was earlier studied for its inorganic geochemical sediment properties (Ti/Al, Ba/Al, V/Al), the oxygen and carbon isotope composition of the planktonic foraminifer *Globigerinoides ruber* and planktonic foraminiferal assemblages and size properties (Hennekam and de Lange, 2012; Hennekam et al., 2014; Mojtahid et al., 2015). In this study, we explore the potential of using single-chamber Ba/Ca, Mn/Ca, and Na/Ca, analyzed with laser ablation ICP-MS (LA-ICP-MS) in the planktonic foraminifer *Globigerinoides ruber* and in six species of benthic foraminifera (*Bolivina alata, Globobulimina affinis, Gyroidina altiformis, Gyroidina orbicularis, Hanzawaia boueana, Uvigerina peregrina*), as potential proxies for past changes in productivity, oxygenation and salinity during sapropel S1. In addition to contributing to a better constraint of the tested paleoproxies for future paleoenvironmental applications, this study presents a unique coupled planktonic-benthic foraminiferal dataset of laser-ICPMS elemental ratios performed on single species from the eastern Mediterranean and during a sapropel event.

2. Material and methods

2.1. Core location and oceanographic settings

Piston core PS009PC (32°07.7′N, 34°24.4′E, 552 m water depth, 690 cm length) was recovered from the SE Levantine Sea in the Nile shore-parallel mud-belt during the PASSAP cruise with the R/V Pelagia (May–June 2000). The core was retrieved from a topographic elevation in order to avoid possible turbidite pathways and effects of downslope transport (Hennekam et al., 2014) (Fig. 1a). At this location, sediments are composed mainly of smectites sourced from the Nile River (Hamann et al., 2009) with a flux estimated at 120×10^6 t a^{-1} for the pre-Aswan modern times (Revel et al., 2010 and references therein). Nile-derived suspended fine sediments and freshwater are transported to our core location by means of the counterclockwise surface circulation of the eastern Mediterranean basin.

In terms of oceanographic setting, and as shown by the CTD cast performed in August 1999 during the cruise Smilable, the SE Levantine Sea comprises three main water masses (Fig. 1b). (1) The Modified Atlantic Water (MAW) is present in the surface 50 to 200 m and consists of a mixture of highly saline Levantine Surface Water and less saline Atlantic Water (Manca et al., 2004; UNEP/MAP, 2012). This water mass increases in salinity with increasing evaporation to the east with a maximum of 38 – 39 PSU in the Levantine basin (Wüst, 1961; Kress et al., 2014). Temperatures vary from ~17°C in winter to ~28°C in summer (Marullo et al., 1999). (2) The Levantine intermediate water (LIW) between 200 and 600 m water depth is characterized by temperatures of ~15.5°C and salinities of ~39.1 (Kress et al., 2014). LIW is formed in the Rhodes gyre in winter, as a result of downwelling of the saline MAW after being cooled down by northern winds (UNEP/MAP, 2012). (3) The eastern Mediterranean Deep Water (EMDW), which fills up the deeper part of the basin, is cooler (~13.5°C) and less saline (~38.7) than the LIW (Kress et al., 2014).

2.2. Age model

For an accurate comparison between the proxies measured in core PS009PC, we use the same age model as published in Hennekam et al. (2014) and Mojtahid et al. (2015). In short, the age model is based on eleven ^{210}Pb and seven ^{14}C data. The ^{14}C analyses were performed on approximately 10 Mg of planktonic foraminifer tests of different species. Accelerator Mass Spectrometry (AMS) ^{14}C ages were converted to calendar ages (years before present, BP) using the depositional model provided by OxCaL 4.1.7 (Ramsey, 2009) based on the Marine09 radiocarbon calibration curve (Reimer et al., 2009) after applying a 21 year local reservoir correction. Following the age model, a sedimentation rate of ~12 cm/ka was recorded during sapropel S1.

2.3. Sedimentary geochemical analyses

The bulk inorganic analyses for Al, Ba, V and Mn were made by X-ray fluorescence using glass beads at the Institute of Chemistry and Biology of the Marine Environment (ICBM) in Oldenburg with a Philips

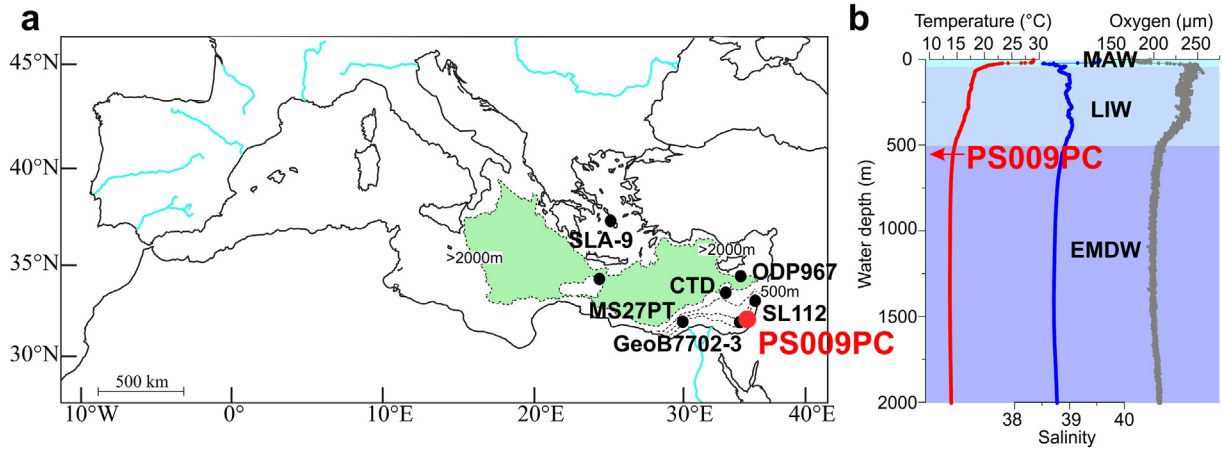

Fig. 1. a) The Mediterranean Sea. The green area in the eastern Mediterranean Sea depicts the depths > 2 km that were nearly continuously anoxic during sapropel S1 formation (De Lange et al., 2008). Core PS009PC (red, this study) is indicated; other relevant sites discussed in the text are also indicated; b) Typical water column profiles of temperature (red), salinity (blue), and dissolved oxygen (grey) in this area from a CTD cast (location visible in (a), taken in August 1999 during the cruise Smilable, PI: Gert de Lange) in the Levantine Basin. The water masses of Modified Atlantic Water (MAW, cyan), Levantine Intermediate Water (LIW, light blue) and Eastern Mediterranean Deep Water (EMDW, blue) are shown. The arrow shows the depth of core PS009PC in this water column profile, at the transition zone between LIW and EMDW.

PW 2400 X-ray spectrometer. For total organic carbon content (Corg), the samples were decalcified using 1 M hydrogen chloride, and were subsequently measured with a Fisons type NA 1500 NCS elemental analyzer (See Hennekam et al. (2014) for detailed methodology). All results reported here were published in Hennekam et al. (2014) except for Mn/Al.

2.4. Foraminiferal-based analyses

2.4.1. Stable oxygen and carbon isotopes

Approximately 20–30 specimens for the planktonic foraminifer *Globigerinoides ruber* (white) and ~5–10 specimens for each of the benthic foraminifera *Uvigerina peregrina* and *Uvigerina mediterranea* were manually selected from the 250–300 µm and > 250 µm fractions, respectively. For *G. ruber*, $\delta^{18}O$ and $\delta^{13}C$ were performed at a 1-cm resolution (average of ~74 yr per sample; 95 samples from ~5 to 12 cal ka BP), and at a 4-cm resolution (average of ~296 yr per sample) for the benthic species provided there were enough tests for one measurement (21 samples with at least one of the two species from ~5 to 12 cal ka BP). The methodology and the results of $\delta^{18}O$ and $\delta^{13}C$ of *G. ruber* are published in Hennekam et al. (2014) and Mojtahid et al. (2015), respectively. In order to correct for the global effect of glacio-eustatic changes on the $\delta^{18}O_{G.\ ruber}$ record and therefore isolate local climatic effects (e.g. Nile freshwater input), we calculated the $\delta^{18}O$ 'residuals' beyond 68% lower confidence limit following the method described in Grant et al. (2016). For the benthic $\delta^{18}O$ and $\delta^{13}C$, cleaning of the foraminiferal samples before mass spectrometry analyses followed the same protocol as for *G. ruber* (i.e. cleaning with 10% hydrogen peroxide (H_2O_2) then methanol (CH_3OH); Hennekam et al., 2014). The cleaned foraminiferal tests were then crushed and mixed, and an amount of 20–60 µg was weighed before placing it into the Kiel-III carbonate preparation device. After reaction of the carbonate with H_3PO_4, the stable isotope values were measured with the MAT253 mass spectrometer at Utrecht University. Standard deviation of ± 0.04 ‰ for $\delta^{13}C$ and ± 0.06‰ for $\delta^{18}O$ obtained from 48 measurements of the NBS-19 standard. All oxygen and carbon isotope data are reported per mil (‰) relative to the Vienna PeeDee Belemnite.

2.4.2. Single foraminifera ICP-MS analyses

About 25 specimens of the planktonic foraminifer *G. ruber* were picked every 6 to 14 cm (8 samples in total) from ~11.0 to ~5.7 cal ka BP. For benthic foraminiferal analyses, six species (*Bolivina alata*, *Globobulimina affinis*, *Gyroidina altiformis*, *Gyroidina orbicularis*, *Hanzawaia boueana*, and *Uvigerina peregrina*) were selected from every 2 cm (33 samples in total) from ~10.8 to ~5.5 cal ka BP. Depending on the density of benthic foraminifera at each sampled level, an average of five specimens per species and per level were analyzed. The tests were cleaned by addition of ~10% hydrogen peroxide (H_2O_2) for 20 minutes to remove organic matter. The H_2O_2 was removed using a pipette and rinsed three times with double deionized water. Samples were subsequently rinsed with Methanol (CH_3OH) for approximately 10 min. The specimens were then rinsed two more times with double deionized water and dried for at least 24 hours in an active fume hood (50°C). After each rinsing step, samples were ultrasonified.

Foraminiferal Mg/Ca, Ba/Ca, Mn/Ca and Na/Ca were determined using Laser Ablation-Inductively Coupled Plasma-Mass Spectrometry (LA-ICP-MS), performed at the NIOZ (benthic foraminifera) and Utrecht University (planktonic foraminifera). The NIOZ setup consists of a NWR193UC (New Wave Research) LA-system equipped with a two-volume cell (TV2 and iCAP-Q) quadrupole ICPMS (Thermo Fisher Scientific), while the Utrecht University setup consists of a 193-nm wavelength COMPex 102 ArF excimer LA system (Lambda Physik, Göttingen, Germany) connected to an Element 2 ICP-MS (Thermo Scientific, Bremen, Germany). Two chamber of each specimen of *G. ruber* were measured (F-1 and F-2) and each specimen of the six benthic species was measured three times on average in 3 to 4 different chambers' positions. Because of the complex organization of benthic tests, it is challenging to determine the exact chamber's position relatively to the final chamber (F). Therefore, we use the numbers 4 to 1 to represent the ontogenetic stages from the oldest to the youngest (Fig. S1). In total and all levels combined, 239 measurements were performed on G. *ruber* (on average 30 measurements for each sampled level) and 1374 measurements were performed on benthic specimens of the six species (on average 42 measurements for each sampled level). Analyzed masses included ^{23}Na, ^{137}Ba, ^{55}Mn, ^{43}Ca, ^{44}Ca, ^{25}Mg, ^{27}Al, and ^{57}Fe. All laser spots were 60–80 µm in diameter (depending on chamber size), repetition rate was set at 6Hz and laser energy density was set at 1 J cm^{-2}. Time resolved signals were selected for integration, background subtracted, internally standardized to ^{43}Ca, and calibrated against a glass standard (NIST SRM610), using Thermo Qtegra software version 2.2.1465.44 and reference values from Jochum et al. (2011). The glass standard was ablated at a higher energy density (5 J cm^{-2}). Using different ablation energies for glass and calcite was previously shown not to affect the analyses (Wit et al., 2010).

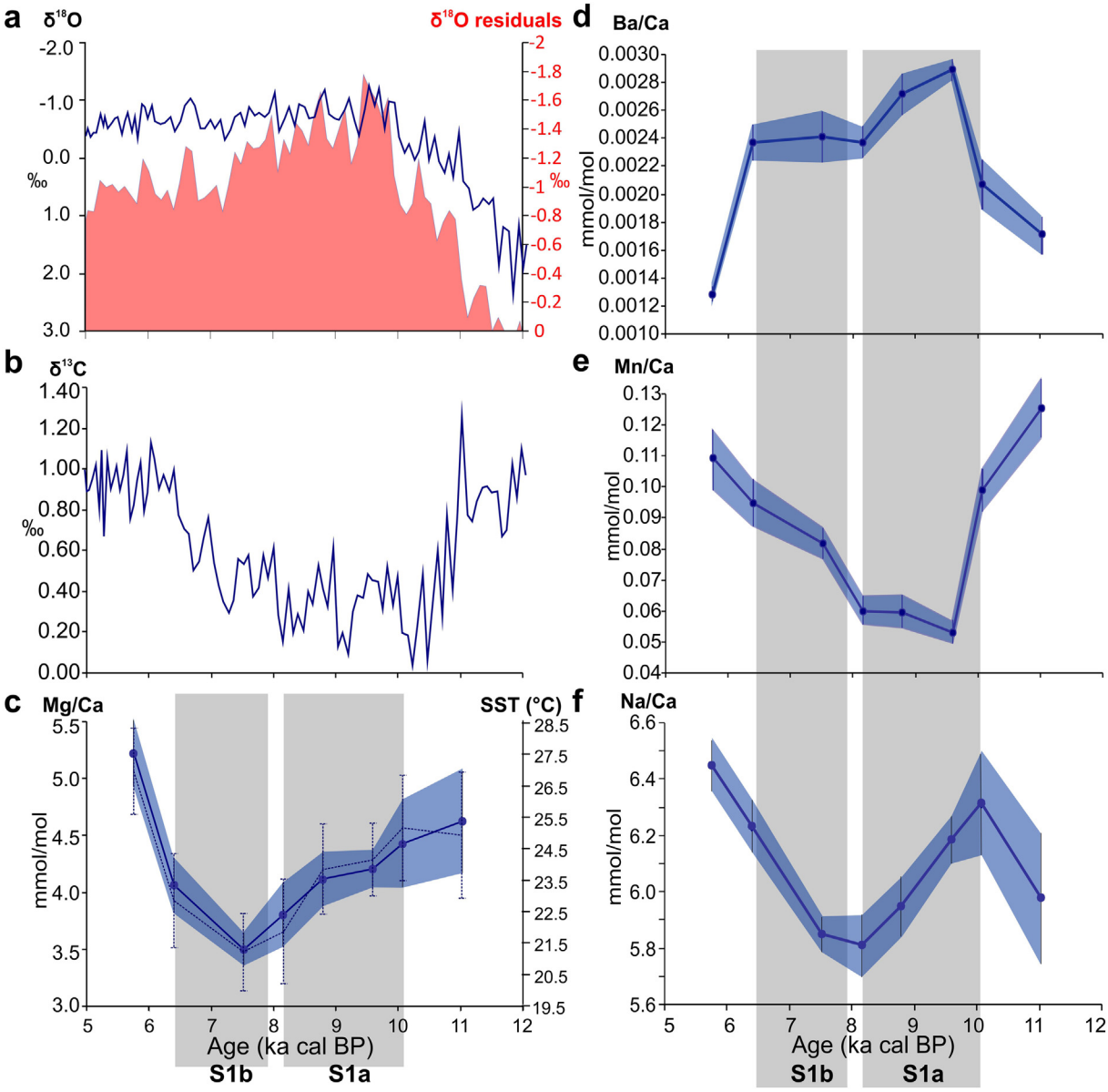

Fig. 2. *G. ruber* results from core PS009PC: a) $\delta^{18}O$ (Hennekam et al., 2014) and $\delta^{18}O$ 'residuals' of *G. ruber* beyond 68% lower confidence limit. Note the conventional glacial-interglacial inversion of the axis values; b) $\delta^{13}C$ of *G. ruber* (Mojtahid et al., 2015); (c-f) El/Ca ratios in mmol/mol. Mg/Ca ratios are corrected for Mg-Mn contamination phase (see text). Each dot represents the average El/Ca values of all measurements performed on *G. ruber* specimens at each sediment level. The colored areas represent the standard errors. Mg/Ca-SST values, presented a dashed blue curve in (c) with a with 1-sigma error, are calculated using the pCO_2 protocol of Gray and Evans (2019).

Integration windows that separate the calcitic signal from background and detection of any contaminants at the test surface were done using Thermo Qtegra software version 2.2.1465.44. Elemental ratios with respect to Ca were based on the average of each ablation profile. The error bars of El/Ca ratios presented in Figs. 2–6 and Fig. S1 represent the standard errors of the means (=RSD/√ n); RSD being the relative standard deviation and n the number of measurements per sediment level and species.

Each laser ablation measurement was screened for contamination and diagenetic surface coatings by monitoring Al, Mn, and Fe. On encountering surficial clay contamination (indicated by Al and Fe peaks) the data integration interval was adjusted to exclude the zone of Al, Mn, and Fe enrichment (if present). However, it has been shown that Mn-rich diagenetic overgrowths are not merely restricted to the test surface but are pervasive throughout the test (e.g. Sexton et al., 2006; Schneider et al., 2017). In that sense, the removal of Mn-rich contaminant phases may have required an additional reductive cleaning step (Boyle and Keigwin, 1985). Here again, it has been suggested to preferentially dissolve Mg-rich biogenic carbonate, potentially introducing an analytical bias in Mg/Ca and possibly in other El/Ca ratios. An alternative way was recently proposed by Hasenfratz et al. (2017) to correct for Mg in the contaminant phase that may occur inside the tests. Indeed, by finding a nearly constant Mg/Mn ratio of ~0.2 mol/mol in the Mn coating of several foraminiferal species from different settings, the following the Eq. (1) can be applied (ox represents the oxidative cleaning procedure):

$$\frac{Mg}{Ca}\text{corrected} = \frac{Mg}{Ca}\text{ox} - \left(\frac{Mn}{Ca}\text{ox} \times \frac{Mg}{Mn}\text{coating}\right) \quad (1)$$

After applying this correction to all our Mg/Ca ratios, the results show only a minor effect of this inner tests Mg-Mn rich overgrowths (~0.2–3.5%) on the final Mg/Ca signature.

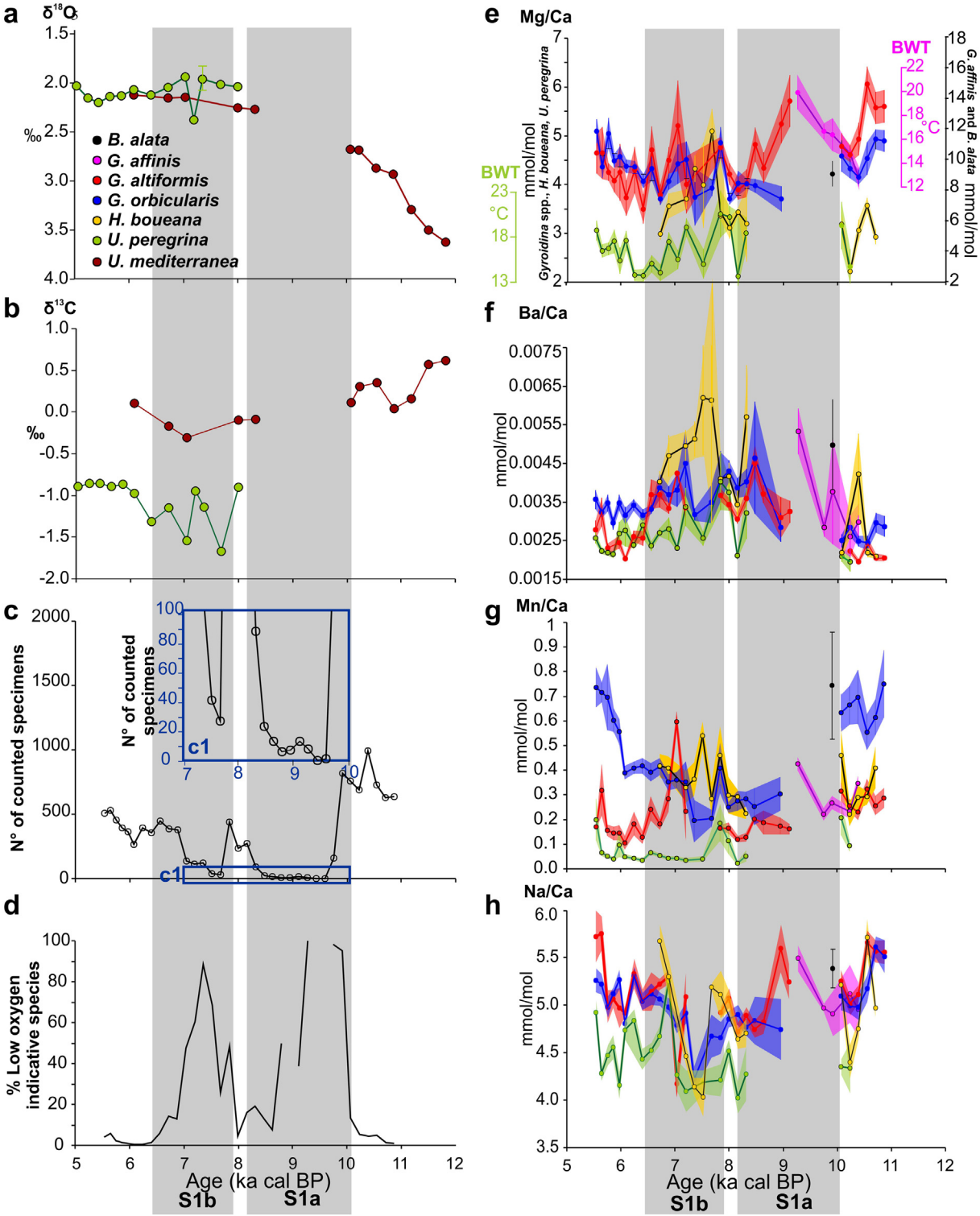

Fig. 3. Benthic foraminiferal results from core PS009PC: a-b) $\delta^{18}O$ and $^{\delta 13}C$ measured on *U. peregrina* and *U. mediterranea*. Note the conventional glacial-interglacial inversion of the $\delta^{18}O$ axis values; c) Absolute densities of benthic foraminifera; d) Cumulative percentages of low oxygen indicative species (*C. bradyi*, *C. oolina*, *F. rotundata* and *G. affinis*); (e-h) El/Ca ratios in mmol/mol measured for six benthic foraminiferal species (*B. alata*, *G. affinis*, *G. orbicularis*, *G. altiformis*, *H. boueana*, and *U. peregrina*). Mg/Ca ratios are corrected for Mg-Mn contamination phase (see text). Each dot represents the average El/Ca values of all measurements performed on all specimens of the same species at each sediment level. The colored areas represent the standard errors. BWT: Bottom water temperatures calculated using the equations of Lear et al. (2002) for *U. peregrina* ($Mg/Ca = 0.924e^{0.061T}$) and Skinner et al. (2003) for *G. affinis* ($Mg/Ca = 2.91e0.080T$).

In order to convert Mg/Ca ratios into water temperatures, we used different calibration equations depending on the species. For *G. ruber* white, we used the pCO_2 protocol of Gray and Evans (2019) (R software package MgCaRB) to correct for pH and salinity effects. Salinity values (S) during sapropel 1 were derived from Emeis et al. (2000) and total alkalinity (A_T) values were derived from the equation of Hassoun et al. (2019) from the eastern Levantine basin for surface waters ($A_T = 27.28*S + 1533.4$). The Mg/Ca bottom water temperatures (T)

are derived from the equation of Skinner et al. (2003) ($Mg/Ca = 2.91e^{0.08T}$) for *G. affinis* and Lear et al. (2002) ($Mg/Ca = 0.924e^{0.061T}$) for *U. peregrina*.

2.4.3. Benthic foraminiferal counts and low oxygen indicative species

From ~5.5 to 10.9 cal ka BP, thirty-seven samples (every 2 cm) were analyzed for their benthic foraminiferal content. Samples were dried and washed over a 150 μm sieve. Benthic foraminiferal specimens were picked under a stereomicroscope, stored in separate Chapman slides (for each sample), and identified at a species level. In this study we only present the total number of counted specimens and the cumulative percentages of low oxygen indicative species (*Cassidulinoides bradyi*, *Chilostomella oolina*, *Fursenkoina rotundata* and *Globobulimina affinis*) as defined by Schmiedl et al. (2010) from the nearby sediment core SL112 (Fig. 1a). To calculate the cumulative percentages, a statistical threshold of 10 individuals was established.

2.5. Time series analyses

In order to explore the frequencies in the temporal variability of selected parameters (Ba/Al_{sed}, V/Al_{sed}, PFAR, $Ba/Ca_{benthics}$), we removed the dominant low-frequency 'precession' peak by applying a band-pass filter stopping wavelengths > 2.6 kyr and analyzed the filtered records using REDFIT analyses. These were performed using the PAST software package (Hammer et al., 2001). Prior to these analyses, data were resampled (i.e. interpolated between data points) at continuous and even spaced time resolution (according to the average time-resolution; Ba/Al_{sed} and V/Al_{sed} = 39 yrs, PFAR = 175 yrs, and $Ba/Ca_{benthics}$ = 170 yrs). To overcome the large intraspecimen and interspecimen variability that is a common feature in all El/Ca ratios, analyses of $Ba/Ca_{benthics}$ were performed on the 2-pt average values of $Ba/Ca_{benthics}$ measurements including all species.

3. Results

3.1. Globigerinoides ruber (white) analyses

The averaged $Mg/Ca_{G.ruber}$ values range from 3.49 ± 0.15 to 5.23 ± 0.30 mmol/mol (Fig. 2c). The $Mg/Ca_{G.ruber}$ record starts with an overall decreasing trend until reaching minimum values at 7.5 cal ka BP, followed by an increase to reach maximum values at ~5.75 cal ka BP (Fig. 2c). The averaged $Ba/Ca_{G.ruber}$ values range from 1.28 10^{-3} ± 8.7 10^{-5} to 2.89 10^{-3} ± 8.0 10^{-5} mmol/mol (Fig. 2d). We observe overall high Ba/Ca values during S1 deposition with a rapid increase from 11.0 to 9.6 cal ka BP followed by a progressive decrease until 6.4 cal ka BP, and thereafter a further decrease until reaching minimum values at 5.75 cal ka BP (Fig. 2d). The average $Mn/Ca_{G.ruber}$ values range from 0.059 ± 0.005 to 0.12 ± 0.009 mmol/mol (Fig. 2e). A rapid decrease in $Mn/Ca_{G.ruber}$ values is recorded from a maximum at 11.0 to a minimum at 9.6 cal ka BP, followed by a gradual increase to reach 0.11 ± 0.009 mmol/mol at 5.75 cal ka BP (Fig. 2e). The average $Na/Ca_{G.ruber}$ values range from 5.80 ± 0.11 to 6.44 ± 0.09 mmol/mol (Fig. 2f). We observe an increase in $Na/Ca_{G.ruber}$ values from ~11.0 to 10.0 cal ka BP, followed by a decrease to reach minimum values at 8.15 ka, and thereafter a general increase is recorded to reach maximum values at ~5.75 cal ka BP (Fig. 2f).

3.2. Benthic foraminiferal analyses

Results of oxygen isotopes ($\delta^{18}O$) measured on the benthic species *U. peregrina* and *U. mediterranea* show a gradual trend from heavy values of ~3.6‰ at 11.8 cal ka BP to more depleted values around 7.0 cal ka BP ($\delta^{18}O_{U.\ peregrina}$ = 1.9‰ and $\delta^{18}O_{U.\ mediterranea}$ = 2.1‰) (Fig. 3a). Thereafter, stable $\delta^{18}O$ values of ~2.1 ‰ are recorded for both species (Fig. 3a). $\delta^{13}C_{Uvigerina}$ spp. show overall low values during S1, with lighter absolute values for *U. peregrina* compared to *U. mediterranea* ($\Delta\delta^{13}C_{U.\ mediterranea\text{-}U.\ peregrina}$ ~1.1 ‰) (Fig. 3b). $\delta^{13}C_{U.\ peregrina}$ values range from a minimum of −1.6‰ at ~7.6 cal ka BP to a maximum of −0.8‰ reached at 8.0 and 5.8 cal ka BP whereas $\delta^{13}C_{U.\ mediterranea}$ values range from a minimum of -0.3‰ at ~7.0 cal ka BP to a maximum of 0.3‰ at 10.5 cal ka BP. We observe a large variability in $\delta^{13}C_{U.\ peregrina}$ during the S1b phase (Fig. 3b). No data are available between 10.0 and 8.3 cal ka BP because of insufficient amounts of *Uvigerina* tests being present in this interval.

The total number of benthic foraminifera range from a minimum of 0 individuals at 9.4 cal ka BP to a maximum of 990 counted specimens (~1644 ind/cm2/ka) at 10.4 cal ka BP (Fig. 3b). Overall low values are present across the S1 deposit with two critical periods (9.6-8.5 and at 7.7 ka cal BP) presenting less than 30 individuals (Fig. 3c). These periods are characterized by a high percentage of low oxygen indicative species (*C. bradyi*, *C. oolina*, *F. rotundata* and *G. affinis*) (Fig. 3d). An interruption at ~8 cal ka BP is observed through an increase in abundances reaching 480 individuals (Fig. 3c), accompanied with a noticeable decrease in the percentage of low oxygen indicative species (Fig. 3d).

Considering all benthic foraminiferal species, $Mg/Ca_{benthics}$ values range from 2.12 ± 0.13 to 14.81 ± 1.12 mmol/mol, with an overall decreasing trend from 11 to 6.5 cal ka BP, followed by increasing values until 5.5 cal ka BP (Fig. 3e). $Ba/Ca_{benthics}$ values range from 1.96 10^{-3} ± 0.11 10^{-3} to 6.19 10^{-3} ± 1.4710^{-3} mmol/mol, with overall high Ba/Ca values during S1 (Fig. 3f). $Mn/Ca_{benthics}$ values vary between 0.02 ± 0.002 and 0.75 ± 0.06 mmol/mol with generally low $Mn/Ca_{benthics}$ ratios during S1 (Fig. 3g). $Na/Ca_{benthics}$ values range between 4.02 ± 0.16 mmol/mol and 5.75 ± 0.17 mmol/mol with an overall decreasing trend from ~11 to 7.5 cal ka BP, followed by increasing values until 5.5 cal ka BP (Fig. 3h). When considering the measured species separately, the record shows significant inter-species differences (Fig. 3e–h). The most systematic difference with respect to all elements (Mg, Ba, Mn, Na) is *U. peregrina* showing significantly lower El/Ca values compared to all other species (Fig. 3e–h; Table 1). *Globobulimina affinis* and *B. alata* show significantly higher Mg/Ca ratios that the other species with values ranging from 8.37 ± 0.82 to 14.81 ± 1.12 and 2.12 ± 0.13 to 6.06 ± 0.36 mmol/mol, respectively (Fig. 3e). El/Ca ratios measured on *G. orbicularis*, *G. altiformis* and *H. boueana* show no significant differences except for $Ba/Ca_{H.\ boueana}$ values being higher and with a larger scatter than for the other species (Fig. 3f), and for Mn/Ca values being very different between *G. orbicularis* and *G. altiformis* (Fig. 3f).

4. Discussion

4.1. Planktonic and benthic foraminiferal tests as reliable geochemical signal carriers during S1 in core PS009PC

In the SE Levantine basin, the planktonic species *Globigerinoides ruber* (white) is abundant throughout S1 in core PS009PC (Mojtahid et al., 2015). This tropical-subtropical symbiont-bearing species tolerates a large salinity gradient (~20-49 PSU; Bijma et al., 1990). As such, it proliferates during sapropels in low-saline and productive surface waters resulting from enhanced Nile River runoff (e.g. Rohling et al., 2004; Hennekam et al., 2014; Weldeab et al., 2014; Grimm et al., 2015; Mojtahid et al., 2015). Benthic foraminifera are nearly continuously

Table 1
The averaged difference between El/Ca ratios in *U. peregrina* and the other benthic species found at the same sediment level.

El/Ca (mmol/mol)	Mg/Ca	Ba/Ca	Mn/Ca	Na/Ca
$\Delta_{U.peregrina\text{-}G.altiformis}$	−1.64	−0.32 10^{-3}	−0.13	−0.53
$\Delta_{U.peregrina\text{-}G.orbicularis}$	−1.67	−0.87 10^{-3}	−0.39	−0.61
$\Delta_{U.peregrina\text{-}H.boueana}$	−0.55	−1.28 10^{-3}	−0.25	−0.53

present across S1 (Fig. 3c), a feature also found in nearby core SL112 (Schmiedl et al., 2010). This implies that either intermittent ventilation or continuous hypoxia prevailed (Casford et al., 2003; Schmiedl et al., 2010). Seafloor anoxia is unlikely due to the shallow position of the core (550 m water depth). That said, an exception can be made for the ~9.6-8.6 cal ka BP time period characterized by extremely low foraminiferal abundances (0–13 specimens; Fig. 3c) and the near exclusive presence of the deep infaunal species *Globobulimina affinis* and *Chilostomella oolina* (Fig. 3d), suggesting that anoxia may have prevailed during this period, also at this depth. However, the surprising near-continuous presence of benthic faunas during S1 leads us to consider whether the ablated specimens are autochthonous or transported. An autochthonous origin is most likely since *Gyroidina orbicularis/altiformis*, *Hanzawaia boueana* and *Uvigerina peregrina* were found as part of several sapropelic foraminiferal successions in the Mediterranean (e.g. Nolet and Corliss, 1990; Casford et al., 2003; Kuhnt et al., 2007; Schmiedl et al., 2010; Triantaphyllou et al., 2016). The water depth of 550 m is a typical depth limit in the eastern Mediterranean for most of the present species (De Rijk et al., 2000), so that reworking from shallower sites would be an unlikely source. Core PS009PC was also retrieved from a topographic elevation, thus largely avoiding possible slumping pathways and other downslope transport features (Hennekam et al., 2014). However, because of the extremely low abundances at ~9.6-8.6 cal ka BP, the autochthonous character of the ablated *G. affinis* and *G. altiformis* at this time interval can be questioned, suggesting that these specimens might be reworked from older samples or nearby settings. Hence, this short period characterized most likely by a severe dysoxia should be interpreted with care, if only for the low numbers of measurements performed compared to the rest of the Sapropel record.

4.2. Surface and deep water conditions during S1 derived from foraminiferal El/Ca

4.2.1. Geochemical signals assessed by the conventional foraminiferal-based proxies $\delta^{18}O$, $\delta^{13}C$ and Mg/Ca

The most conventional foraminiferal-based proxies ($\delta^{18}O$, $\delta^{13}C$) measured on *G. ruber* and *Uvigerina* spp. in core PS009PC show the expected patterns for surface and deep water characteristics during S1 (Figs. 2a–c; 3a–b). Hennekam et al. (2014) argued that the depleted $\delta^{18}O$ signal of *G. ruber* during S1 (Fig. 2a) is closely linked to Nile River discharges. After correcting for the effect of glacio-eustatic sea-level changes (Rohling et al., 2014; Grant et al., 2016), the effect of Nile freshwater inflow can be isolated (Fig. 2a). Furthermore, the enhanced Nile discharge introduced depleted $\delta^{13}C$ terrestrial carbon explaining most of the depleted $\delta^{13}C_{G.\ ruber}$ values during S1 (Fig. 2b) (Grimm et al., 2015; Mojtahid et al., 2015). The $\delta^{18}O$ measured on *Uvigerina* spp. records the expected glacial-interglacial transition similar to the global benthic stack record of Lisiecki and Raymo (2005) and the other eastern Mediterranean records (e.g. ODP967; Ziegler et al., 2010). Likewise, the overall depletion during S1 in $\delta^{13}C_{Uvigerina\ spp.}$ (Fig. 3b) is similar to other Mediterranean benthic records implying significantly higher residence times of deep-water masses and/or higher influx of terrestrial dissolved organic carbon via enhanced river runoff (e.g. Kuhnt et al., 2008; Schmiedl et al., 2010; Grimm et al., 2015). The ~1.1 ‰ difference between $\delta^{13}C_{U.\ peregrina}$ and $\delta^{13}C_{U.\ mediterranea}$ has been reported before and can be explained partly by the "vital effect" and the microhabitat preferences within the sediment (see review in Ravelo and Hillaire-Marcel, 1999; Fontanier et al., 2006).

In our record, sea surface temperatures (SST) vary between ~21.24 ± 1.36 and 27.00 ± 1.23 °C (Fig. 2c). These values are overall within the range of SST values reconstructed using alkenone unsaturation ratios in the Levantine during S1 (16.7–21.9 °C at ODP967, Emeis et al., 2000, 22.3–24 °C at GeoB 7702-3, Castañeda et al., 2010). However, these studies show that SST either remained stable or slightly increased, which is inconstant with the decrease we record in $Mg/Ca_{G.\ ruber}$ values during S1 (Fig. 2c). For both methods, several effects are known to bias temperature reconstructions. While alkenone paleotemperature determinations suffer from seasonality and water depth biases (e.g. Castañeda et al., 2010; Tierney and Tingley, 2018), foraminiferal-based Mg/Ca SST reconstructions can be affected by diagenesis, salinity and pH amongst others (e.g. Gray et al., 2018; Gray and Evans, 2019). In our samples, the insignificant difference (~0.2 - 3.5%) between the measured Mg/Ca and the corrected ratios (Hasenfratz et al., 2017), and the lack of a statistically significant correlation between Mg/Ca and Mn/Ca ratios seem to indicate a minor diagenetic effect. However, in such environmental setting, these arguments might be insufficient to assert a complete absence of such diagenetic effect. Based on eastern Mediterranean Sea core top sediments, several studies show that foraminiferal trace elements are diagenetically altered by post-depositionally precipitated high Mg carbonate calcites, most likely induced by oversaturation of carbonate ion concentration and high salinity (e.g. Ferguson et al., 2008; Hoogakker et al., 2009; Dueñas-Bohórquez et al., 2009; Kontakiotis et al., 2011). This is therefore consistent with an oversaturation-induced diagenesis leading to high Mg/Ca and Mn/Ca in *G. ruber* (Fig. 2c–e) before and after the episode of runoff-induced (i.e. low salinity) S1 formation. Salinity itself is also known to affect the incorporation of Mg into foraminiferal calcite (e.g. Dueñas-Bohórquez et al., 2009; Dissard et al., 2010; Wit et al., 2010; Hönisch et al., 2013). This effect can be expected during S1, a period known for a large shift in surface salinity. When applying a sensitivity of ~3%/PSU (Hönisch et al., 2013; Gray et al., 2018), our $Mg/Ca_{G.\ ruber}$ (3.5–5.2 mmol/mol) results in an improbable ~16 PSU change, where literature in the area report 2 - 4 PSU drop in surface salinity during S1 (Kallel et al., 1997; Emeis et al., 2000). Other factors such as the carbonate system (e.g. Gray et al., 2018) or the $[Mg^{2+}]$ of seawater itself can be also accounted for. For instance, it has been shown that the contribution of the Mg-rich Ethiopian basaltic sediments (i.e. Blue Nile) to the Nile delta were higher compared to present and progressively decreased from 12 to 5 ka cal BP (Fig. 5c; Revel et al., 2014).

For benthic species, the Mg/Ca-derived bottom water temperatures are 17 ± 2.3 °C on average for *G. affinis* (Skinner et al., 2003) and 17 ± 2.6 °C for *U. peregrina* when using the exponential equation of Lear et al. (2002) (Fig. 3e). These temperatures reconstructions are reasonable when compared to the present value of ~15 °C at 550 m depth (Fig. 1b). However, note that most of the other calibrations available for *Uvigerina* genus (see review in Elderfield et al., 2010) give unrealistically warm BWT's when applied to our data, highlighting perhaps significant inter and intra-species differences within the genus (Elderfield et al., 2010). Furthermore, there appears to be an overall drop in benthic Mg/Ca during S1 (Fig. 3e) that resembles that of bottom water salinities modeled by Rohling (1994) (Fig. 6e). Here again, several possible sources of biases, amongst which the salinity effect, are probably hampering the use of Mg/Ca as a precise paleo-thermometer in our study area and time-period.

4.2.2. Sapropel characteristics as derived from foraminiferal Ba/Ca ratios

The general trend of $Ba/Ca_{G.\ ruber}$ is consistent with the results of Weldeab et al. (2014) from the nearby core SL112, although with slightly higher absolute values in our study (Fig. 4a–b). This difference might be due to the use of two different forms of *G. ruber,* the white form in our study and the pink form in the study of Weldeab et al. (2014). These authors argue that the enhanced input of Ba^{2+}-enriched Nile freshwaters during S1 served as an additional local source of Ba^{2+} to the Levantine (e.g. Bahr et al., 2013; Weldeab et al., 2014). In our samples, the close link between $Ba/Ca_{G.\ ruber}$ and Nile River discharges is corroborated by the comparable trend of $\delta^{18}O_{G.\ ruber}$ 'residuals' tracing Nile freshwater input (Fig. 4b). Hence, we interpret the variation of $Ba/Ca_{G.\ ruber}$ to primarily reflect changes in Nile River discharge and so humidity changes over the Nile basin (Weldeab et al., 2014).

Benthic foraminiferal Ba/Ca ratios plot within the normal observed ranges of "small" benthic foraminiferal (i.e. opposed to tropical "large" benthic foraminifera) shell abundances (e.g. Lea, 1999;

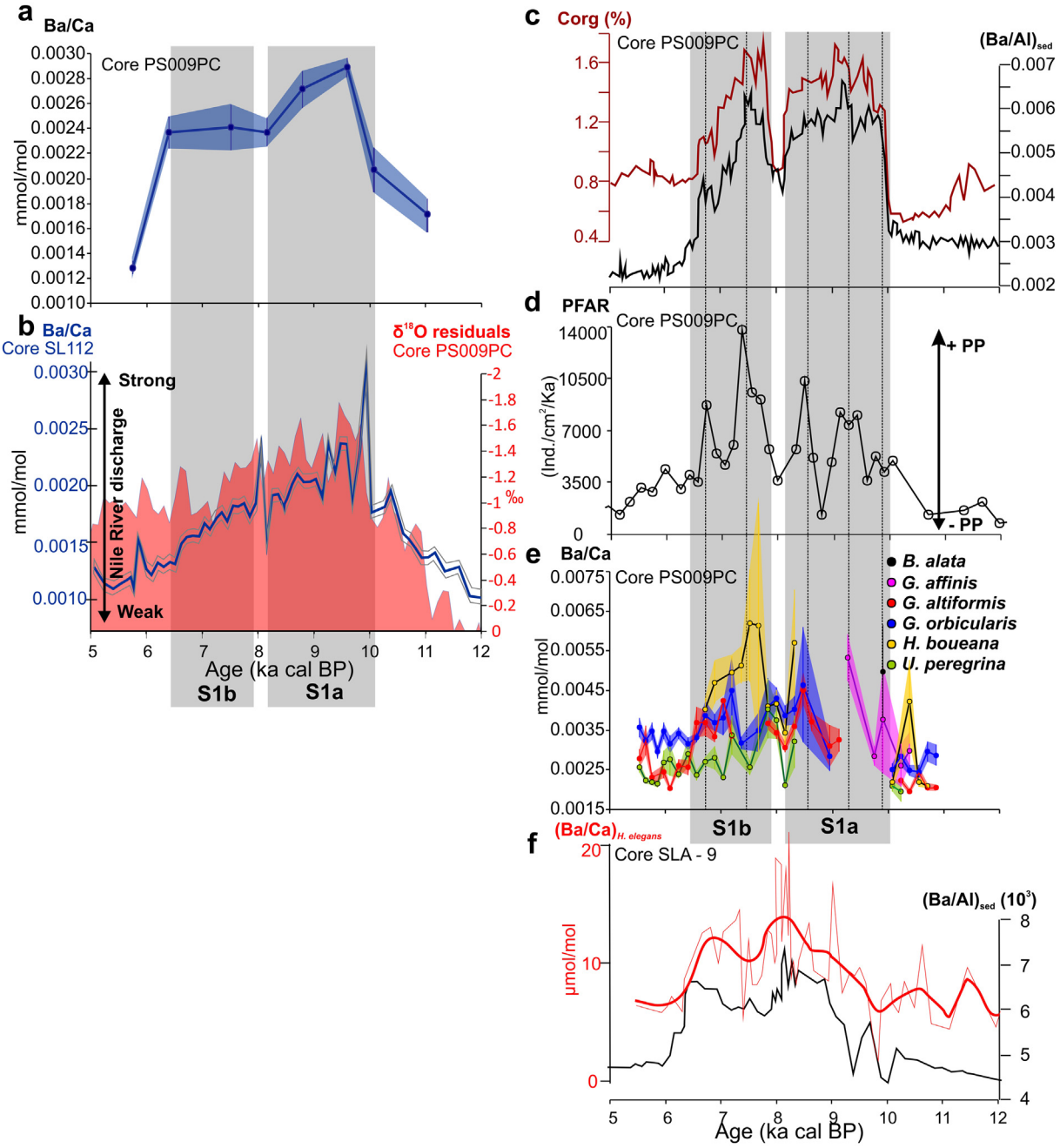

Fig. 4. a) Ba/Ca$_{G.\ ruber}$ from core PS009PC; b) Ba/Ca$_{G.\ ruber}$ from core SL112 (Weldeab et al., 2014) and $\delta^{18}O$ residuals of *G. ruber* from core PS009PC. Note the conventional glacial-interglacial inversion of the $\delta^{18}O$ axis values; c) Organic carbon content (Corg) and XRF-(Ba/Al) ratio in the sediment (Ba/Al$_{sed}$) in core PS009PC (Hennekam et al., 2014); d) Planktonic foraminiferal accumulation rates (PFAR) from core PS009PC (Mojtahid et al., 2015). PP: Primary production; e) Ba/Ca ratios in mmol/mol for the six measured benthic foraminiferal species from core PS009PC. Each dot represents the average El/Ca values of all measurements performed on all specimens of the same species at each sediment level. The colored areas represent the standard errors; f) Ba/Ca ratios in µmol/mol measured on the benthic foraminiferal species *Hoeglundina elegans* and XRF-(Ba/Al) ratio in the sediment (Ba/Al$_{sed}$) from core SLA-9 (Ní Fhlaithearta et al., 2010). Thick red line represents 500 year Gaussian smoothing of (Ba/Ca)$_{H.elegans}$ data.

0.0015–0.005 mmol/mol) (Fig. 4e). The overall high Ba/Ca$_{benthics}$ values during S1 are simultaneous to high values of known paleo(export) productivity proxies from the same PS009PC core (i.e. Ba/Al$_{sed}$, organic carbon content-Corg, planktonic foraminiferal accumulation rates-PFAR; Fig. 4) (e.g. Thomson et al., 1999; Mercone et al., 2000; De Lange et al., 2008; Jilbert et al., 2010; Hennekam et al., 2014; Mojtahid et al., 2015). Therefore, the observed simultaneous increase in sedimentary Ba and incorporated Ba in benthic foraminiferal tests indicates a close coupling between Ba/Ca$_{benthics}$ and export productivity during S1 in the SE Levantine Basin. The same conclusions are drawn by Ní Fhlaithearta et al. (2010) from Ba/Ca ratios measured on *Hoeglundina elegans* in core SLA-9 from the Aegean Sea (Fig. 4f). However, many additional factors may affect the Ba integrated in benthic foraminiferal calcite and hence explain part of the variability reported here. For instance, the decrease in surface salinities during S1 may have decreased slightly $BaSO_4$ precipitation (~8% at most for a salinity decrease of 2–4 units; Ní Fhlaithearta et al., 2010) by reducing complexation and increasing the release of free Ba^{2+} (e.g. Millero and Schreiber, 1982). However, this effect was probably limited because Ba/Ca$_{benthics}$ and Ba/Al$_{sed}$ were ~2–3 times higher during S1 relative to the background values (Fig. 4).

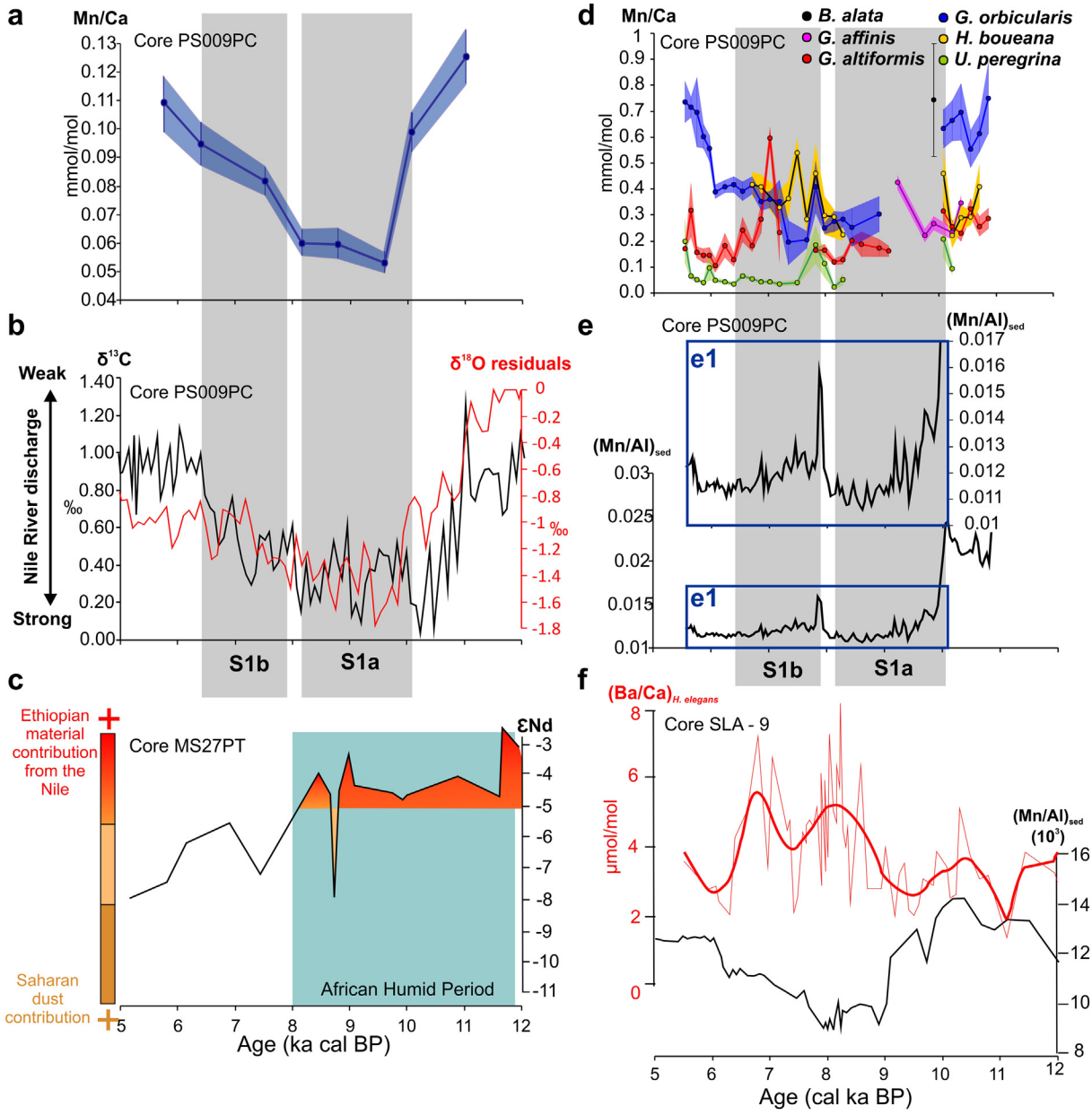

Fig. 5. a) Mn/Ca ratios in mmol/mol measured on *G. ruber* from core PS009PC; b) $\delta^{13}C$ and $\delta^{18}O$ 'residuals' measured on *G. ruber* from core PS009PC; c) Radiogenic $^{143}Nd/^{144}Nd$ (εNd) measured on the terrigenous fraction (< 63 μm) after removal of the biogenic components in core MS27PT (Revel et al., 2014); d) Mn/Ca ratios in mmol/mol of the six measured benthic foraminiferal species from core PS009PC. Each dot represents the average El/Ca values of all measurements performed on all specimens of the same species at each sediment level. The colored areas represent the standard errors; e) XRF-(Mn/Al) ratio in the sediment in core PS009PC (Hennekam et al., 2014); f) Mn/Ca ratios in μmol/mol measured on the benthic foraminiferal species *Hoeglundina elegans* and XRF-(Mn/Al) ratios in the sediment from core SLA-9 (Ní Fhlaithearta et al., 2010). Thick red line represents 500 year Gaussian smoothing of $(Ba/Ca)_{H.\ elegans}$ data.

Alternatively, enhanced $Ba/Ca_{benthics}$ could be related to reduced bottom water ventilation, leading to increased residence time of deeper water Ba^{2+} (Ní Fhlaithearta et al., 2010). We also note important inter-species differences (Fig. 4e) which are nonetheless common for all El/Ca ratios among benthic foraminifera and are probably the result of a combination of several effects which are not yet well constrained (e.g. calcification rate and ontogenetic effects, different biomineralization mechanisms, diagenesis and dissolution effects, microhabitat effect, etc) (e.g. Hintz et al., 2006 and references therein; de Nooijer et al., 2017). In our samples, *U. peregrina* and *H. boueana* systematically yield respectively lower and higher Ba/Ca values that the other species (Fig. 4e). McCorkle et al. (1995) excluded pore water effects for Ba/Ca ratios and proposed long time scale calcite recrystallization and/or dissolution effect as possibly substantially lowering Ba/Ca ratio for some species.

4.2.3. Sapropel characteristics as derived from foraminiferal Mn/Ca ratios

The overall high values of $Mn/Ca_{G.\ ruber}$ ratios (0.05–0.12 mmol/mol; Fig. 5a) are unexpected as dissolved Mn is very low in surface waters (few nmol/L; e.g. Statham and Burton, 1986). Mn/Ca in living and recent planktonic foraminifera are typically well below 0.05 mmol/mol (e.g. Boyle, 1983; Russell et al., 1994; Eggins et al., 2003; Barker et al., 2003). This suggests that in our case, either (i) surface waters were enriched in Mn and/or (ii) most of the Mn is of post-depositional origin. (i) During the African Humid Period (~11.0–8 cal ka BP; Revel et al., 2014) and until the end of S1, Mn may have originated from both atmospheric input of Saharan dust and/or Nile River discharge or re-cycling from deeper anoxic/dysoxic water. These multiple sources may

have enriched the Mn^{2+} pool in the eastern Mediterranean surface waters compared to present. Nonetheless, within the range of the overall high $Mn/Ca_{G.\ ruber}$ values, we observe a clear decrease during S1 that parallels the dynamics of Nile River discharges (Fig. 5a–b). This pattern might result from the relative decline in dust input into the Levantine during a period of greening of the Sahara (e.g. deMenocal et al., 2000), as shown by the εNd signature in the nearby MS27PT core sediments (Fig. 5c; Revel et al., 2014). (ii) The high values of $Mn/Ca_{G.\ ruber}$ may also be indicative of the presence of diagenetic Mn oxyhydroxides inside the test (e.g. Boyle, 1983; Lea, 1999; Barker et al., 2003). As such, the lower $Mn/Ca_{G.ruber}$ values recorded during S1 relative to before and after (Fig. 2e) may suggest a lower precipitation of Mn-oxides due to prevailing low-oxygen conditions.

In PS009PC and the nearby core SLA-9, the release of Mn^{2+} into pore and bottom waters is reflected by the depleted sedimentary Mn (Mn/Al_{sed}) during S1 (Fig. 5e–f). The major interest of measuring Mn/Ca in foraminifera is that, unlike the reactive Mn/Al_{sed}, Mn concentration remains fixed once the foraminiferal calcite precipitated (Koho et al., 2015; McKay et al., 2015). Here again, $Mn/Ca_{benthics}$ values are higher (~0.1–0.8 mmol/mol; Fig. 5d) than the typical range of living and recent benthic foraminiferal calcite (< 0.001–0.15 mmol/mol) (e.g. Boyle and Keigwin, 1985; Lea, 1999; Glock et al., 2012), probably for the same reasons as mentioned for *G. ruber*. Also, a significant positive correlation is found between Mn/Al_{sed} and Mn/Ca measured on *G. altiformis*, *G. orbicularis* and *U. peregrina*, which might indicate that during S1, less Mn-oxides precipitated on benthic foraminifera because of the low oxygen conditions. Additionally, there is a large variability in Mn/Ca values and trends recorded by our six benthic species (Fig. 5a). This can be either due to microhabitat preferences between the different species that calcify in different pore waters (e.g. Koho et al., 2017) or to diagenetic processes resulting in heterogeneous Mn distribution between and within tests (e.g. Klinkhammer et al., 2009; Glock et al., 2012).

4.2.4. Sapropel characteristics as derived from foraminiferal Na/Ca ratios

Recent calibrations based on cultured and field-collected *G. ruber* show that Na incorporation into shell calcite increases with salinity (e.g. Allen et al., 2016; Mezger et al., 2016), albeit that these trends are lost in the sediment (Mezger et al., 2018). In our case study, the overall decrease in $Na/Ca_{G.\ ruber}$ during S1 is coherent with excess Nile River runoff decreasing the surface salinity of the Levantine basin (Emeis et al., 2000) (Figs. 6a–c). After applying the *G. ruber* (white) calibration equation of Mezger et al. (2016) (Na/Ca = 0.57S–12.38), the reconstructed surface salinities in our record range from ~31.9 to 33.0 PSU (Fig. 6a). Pioneer studies suggest a decrease of up to 4.0 units from present (~39; Fig. 1b) (e.g. Vergnaud-Grazzini et al., 1977; Cita et al., 1977; Mangini and Schlosser, 1986), a result corroborated by Kallel et al. (1997) through modeling. More recently, by using residual variations of $\delta^{18}O_{G.\ ruber}$ after temperature and ice volume correction in a deep-sea core south of Cyprus (ODP967), Emeis et al. (2000) report a decrease of about 2.0 units compared to modern surface salinity (Fig. 6c). Therefore, our $Na/Ca_{G.\ ruber}$-derived salinity estimates using the calibration equation of Mezger et al. (2016) appear to underestimate both the absolute values and the net salinity drop (1.0 vs. 2.0 to 4.0 units drop in the literature). The established large impact of carbonate preservation (Mezger et al., 2018, 2019) from sapropel to non-sapropel conditions likely interferes with a straightforward interpretation. The very few studies tackling the use of Na/Ca on planktonic foraminifera as a potential salinity proxy face many constraints that currently hamper its quantification. For instance, recent studies show that Na is enriched in the spines of *G. ruber* and that the loss of spines during settling of foraminifera through the water column might explain some of the variability (Mezger et al., 2018, 2019). In our data, we observe that minimum $Na/Ca_{G.\ ruber}$ values (Fig. 6a) do not coincide with maximum Nile runoff as traced by $Ba/Ca_{G.ruber}$ and $\delta^{18}O$ residuals (Fig. 6b), but rather coincides with minimum $Mg/Ca_{G.ruber}$ (Fig. 2c) ($R^2_{Na/Ca\text{-}Mg/Ca} = 0.56$). This suggests that other processes than salinity are involved in Na/Ca incorporation. For instance, some studies report that high-Mg bands in foraminiferal calcite coincide with elevated concentrations of organic molecules (e.g. Na, S), which were linked to the proximity of organic linings (e.g. Erez, 2003; Geerken et al., 2018). More recently, Mezger et al. (2019) showed that the Na values measured on the isolated linings indicate only a negligible relative contribution to the overall shell Na/Ca.

Na/Ca measured on benthic foraminifera show overall low values during S1 (Fig. 6d) which might reflect a decrease in bottom water salinities. Because most sapropels were devoid of benthic microfossils, only very few estimates of past bottom water salinities are available for S1 at comparable water depths. By using an ocean general model to simulate the thermohaline circulation in the eastern Mediterranean during S1 deposition, Rohling (1994) and Myers et al. (1998) show a reduction in salinity at 450-500 m water depth during S1 attaining ~37.4 (Fig. 6e). This confirms the potential of $Na/Ca_{benthics}$ proxy as a tracer of past bottom water salinities. In order to estimate quantitatively past salinities, we applied for the six benthic species the Na/Ca-salinity calibrations for the intertidal benthic species *Ammonia tepida* of Wit et al. (2013) (Na/Ca = 0.22S–0.75) and of Geerken et al. (2018) (Na / Ca = 0.064S + 3.29). This correction results in both cases in unrealistic bottom waters salinities (~22.0–28.6 and 11.4–38.4 PSU, respectively) compared to the literature (~37.4–41.0) (Figs. 6d-e). As for *G. ruber*, several biases may explain this result. The active precipitation of calcite by foraminifera, as living organisms, argues for significant biological or kinetic controls on trace element substitution, so that El/Ca signature is species specific and so should be the calibration equations (e.g. Lea, 1999; Toyofuku et al., 2000; Geerken et al., 2018). This is highlighted in our results by the differences in Na/Ca values between the six studied benthic species (Fig. 6d).

4.3. What processes during Sapropel 1 formation can be drawn from El/Ca proxies?

Despite the numerous limitations that may question at present the reliability of benthic foraminiferal Ba/Ca, Mn/Ca and Na/Ca ratios as paleo-proxies, the uniqueness of the present study's $El/Ca_{benthics}$-dataset justifies the following attempt to uncover the environmental signal hidden behind these biases. Amongst the three tested El/Ca proxies, $Ba/Ca_{benthics}$ appears to be the most reliable one, because the increase in $Ba/Ca_{benthics}$ during S1 is coherent with increased sedimentary Ba/Al and hence with the expected enhanced productivity as shown also by the PFAR values (Mojtahid et al., 2015) (Fig. 7). In our core study and throughout S1, Hennekam et al. (2014) report that export productivity (Ba/Al) and bottom water redox conditions (V/Al) vary simultaneously with Nile discharge ($\delta^{18}O_{G.\ ruber}$) on multicentennial time scales with a significant cyclicity in the 500–1000 yr band. This is supported by Casford et al. (2003) who hypothesized, through observations of oxyphilic benthic foraminifera from the Aegean Sea and offshore Libya, the possibility of multiple interruptions (without precision on their duration and frequency) in the anoxia occurring throughout sapropels deposition.

In order to assess if such cyclicity is recorded by our foraminiferal productivity indicators, we band-pass filtered (i.e. remove the dominant precession-related sapropel wavelength) selected proxies from core PS009PC: Ba/Al_{sed} and V/Al_{sed} (Hennekam et al., 2014), PFAR (Mojtahid et al., 2015), and the averaged $Ba/Ca_{benthics}$ (Fig. 7). These filtered records show a similar variability (Fig. 7b) with the same significant frequency peaks in the ~1700–2200 yr, 800–1000 yr, and 400–600 yr bands during S1 formation (Fig. 7c). The ~1700–2200 yr peak is probably associated to the well-known 8.2 kyr-event, interrupting S1 (e.g. Rohling et al., 2002; Tachikawa et al., 2015). Internal processes, such as a more pronounced Siberian high-pressure system involving winter cooling in the northern high latitudes (e.g. Pross et al., 2009; Schmiedl et al., 2010; Triantaphyllou et al., 2016), and a

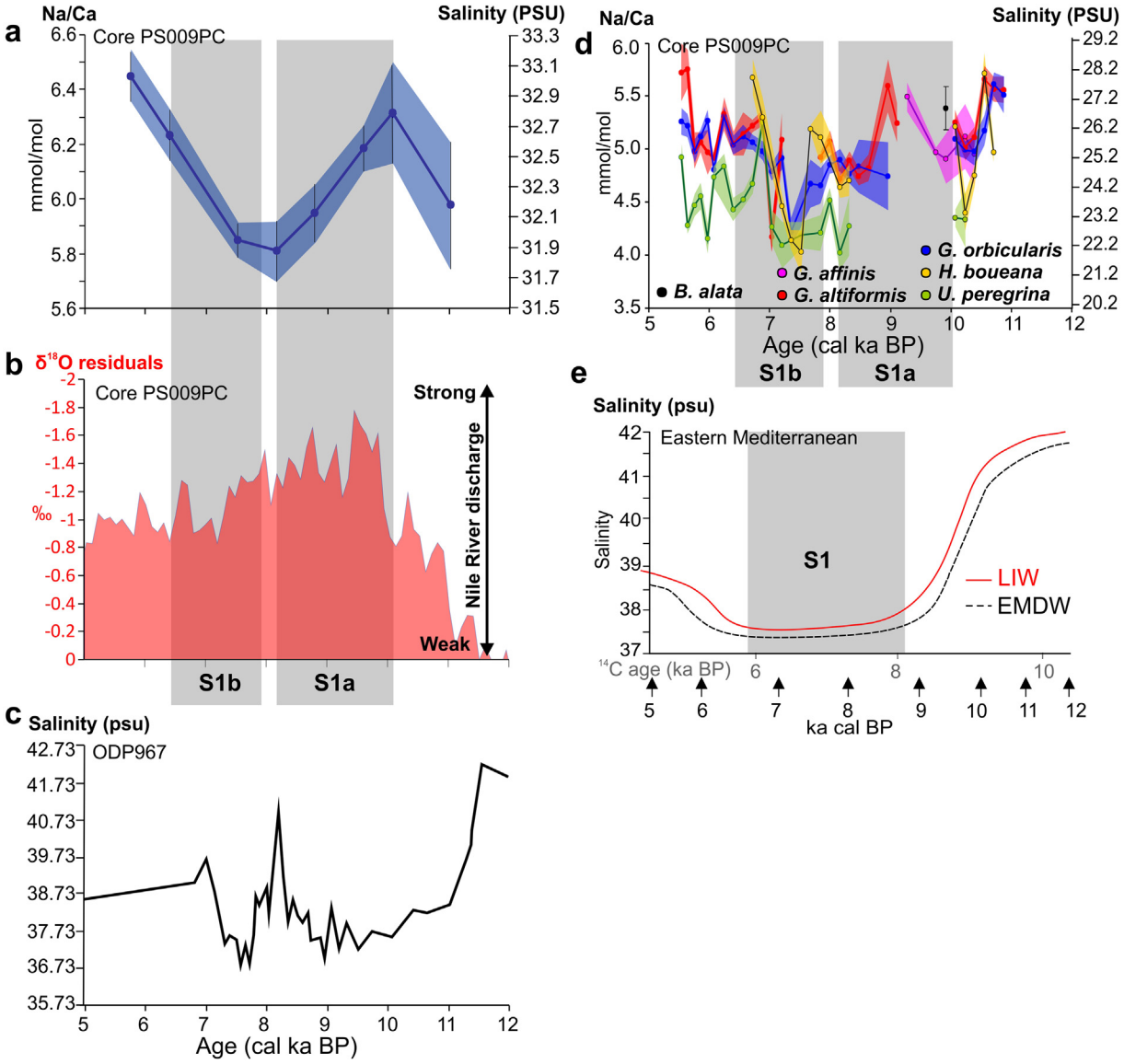

Fig. 6. a) Na/Ca of *G. ruber* from core PS009PC. Salinities are reconstructed using the equation of Mezger et al. (2016) (Na/Ca = 0.57S-12.38); b) $\delta^{18}O$ residuals of *G. ruber* from core PS009PC; c) Surface salinities calculated from $\delta^{18}O_{G.ruber}$ corrected for temperatures using the alkenone unsaturation index UK'37 (Emeis et al., 2000). d) Na/Ca ratios in mmol/mol for the six measured benthic foraminiferal species from core PS009PC. Salinities are reconstructed using the equation of Wit et al. (2013) (Na/Ca = 0.22S-0.75). Each dot represents the average El/Ca values of all measurements performed on all specimens of the same species at each sediment level. The colored areas represent the standard errors; e) Schematic representation of changes in the salinity of S1 analogues of modern LIW (Levantine Intermediate Water) and EMDW (Eastern Mediterranean Deep Water) as constrained by salinity estimates derived from oxygen isotope studies in the Eastern Mediterranean (Rohling, 1994; Myers et al., 1998).

southward migration of the intertropical convergence zone weakening the monsoon systems (e.g. Fleitmann et al., 2007; Triantaphyllou et al., 2009) have been proposed to cause the 8.2 interruption during S1 formation. The ~800–1000 yr, and 400–600 yr peaks describe a multicentennial variability. Hennekam et al. (2014) show that the multicentennial variability observed in PS009PC $\delta^{18}O_{G.\ ruber}$, Ba/Al and V/Al records is strongly resembling the atmospheric $\Delta^{14}C_{res}$ variability (Stuiver et al., 1998) which mainly reflects changes in the strength of the solar activity (Stuiver and Braziunas, 1993). This corroborates a multicentennial time scale control of solar forcing on Nile discharges, productivity and deep-sea ventilation (Hennekam et al., 2014), superimposed on the 21 ka-orbitally induced solar insolation cycle responsible for sapropel deposits (Rossignol-Strick et al., 1982; Rohling, 1994). Solar forcing may act on Nile discharges through the modulation of the southwest Indian summer Monsoon (Hennekam et al., 2014). By bringing more nutrients to the Levantine Basin, river input likely influences productivity and thus oxygen consumption through organic matter decay (De Lange et al., 2008). Solar forcing on ventilation and productivity of the eastern Mediterranean during S1 has been also reported for a 3400 m-deep Ionian site, but with higher frequency (100–300 to 300–600 years cycles) (Jilbert et al., 2010). This difference may be partly attributed to the differing climate controls on the hydrology of northern and southern Mediterranean subbasins influenced by high (e.g. Siberian high) and south latitude climate (e.g. Indian summer monsoon, west African monsoon) respectively (Rohling et al., 2002; Jilbert et al., 2010; Hennekam et al., 2014). All in all, these results confirm that, despite the analytical uncertainties, potential biases, imperfect quantitative calibrations and the lower sampling resolution, our foraminiferal-based proxies record fairly well the close multicentennial and millennial coupling between Ba cycling, export productivity, and redox conditions, during S1 in the SE Mediterranean.

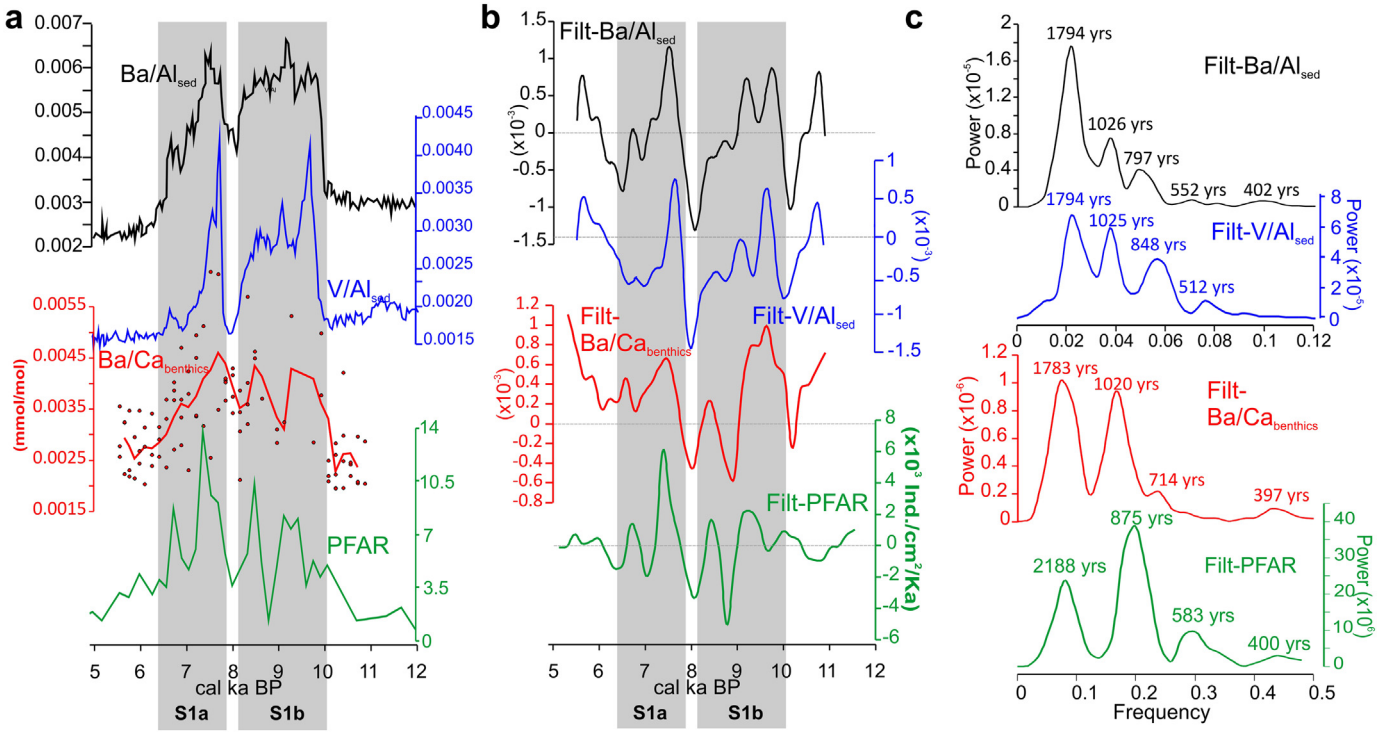

Fig. 7. a) Ba/Al$_{sed}$ and V/Al$_{sed}$ from core PS009PC (Hennekam et al. 2014), 2-pt moving average (red tick line) of Ba/Ca$_{benthics}$ in core PS009PC all benthic foraminiferal species included (each dot represents the average El/Ca values of all measurements performed on all specimens of the same species at each sediment level), and PFAR from core PS009PC (Mojtahid et al., 2015); b) Band-pass filtered records of the same proxies described in (a). All frequencies > 2.6 kyrs were removed; c) REDFIT analyses of the filtered records in (b). All designated frequency peaks are above the theoretical red noise model AR(1).

5. Conclusions

This study provides a unique El/Ca-dataset measured on planktonic and benthic foraminifera from the SE Mediterranean. The study of the well-constrained sapropel S1 period allowed us to evaluate the robustness of newly developed proxies (Ba/Ca, Mn/Ca, Na/Ca). We draw the following key conclusions:

1) Ba/Ca, Mn/Ca and Na/Ca ratios in fossil planktonic and benthic foraminifera follow in many cases the expected surface and bottom water characteristics during S1 formation. Ba/Ca$_{G.\ ruber}$ is a reliable tracer for Ba^{2+}-enriched Nile freshwaters, whereas Ba/Ca$_{benthics}$ track enhanced paleo(export) productivity. The overall decrease in Na/Ca of both planktonic and benthic foraminifera during S1 is coherent with excess Nile River runoff resulting in a decrease in surface and bottom water salinities in the < 500m water column of the Levantine basin. The interpretation of Mn/Ca data is less straightforward, probably because of additional sources of Mn to the Levant during S1, and inner tests Mn-rich overgrowths. Nevertheless, all Mn/Ca ratios show lower values during S1 suggesting a lower precipitation of Mn-oxides under prevailing hypoxic conditions.
2) Although the obtained El/Ca ratios revealed to be promising overall as paleoproxies, several issues arise. These issues are partly linked to their relatively recent development, so that not enough data are available. Amongst these, we show existing strong interspecies differences in all analyzed El/Ca and potential co-variations in elements (e.g. Mg/Ca and Na/Ca). Therefore, there is need for more species-specific calibrations from empirical, in-situ, core-top and culturing approaches in order to correct more precisely for the multiple potential sources of biases.
3) Times series analyses performed on Ba/Ca$_{benthics}$ highlight a multi-centennial variability, in coherency with other paleo(export) productivity (Ba/Al$_{sed}$, PFAR) and redox (V/Al$_{sed}$) proxies from the same studied core. We therefore conclude that benthic foraminiferal Ba/Ca records the close coupling between Ba cycling, export productivity, and redox conditions, during S1 in the SE Mediterranean.

Supplementary data to this article can be found online at https://doi.org/10.1016/j.marmicro.2019.101783.

Acknowledgments

This study is part of a project MADHO (MediterraneAn Deltas in the Holocene) financed by the international program MISTRALS PaleoMEX. The "*Région Pays de la Loire*" is acknowledged for financial support to TANDEM project (PI: M. Mojtahid) involving the 18-month post-doctoral fellowship provided to Sandrine Le Houedec. NWO is acknowledged for financial support to PASSAP cruise and PASS2 and PALM projects. Data to support this article are from University of Angers (France) and University of Utrecht (The Netherlands). The data are available online as supplementary material and/or by contacting the first author (e-mail: meryem.mojtahid@univ-angers.fr).

References

Allen, K.A., Hönisch, B., Eggins, S.M., Haynes, L.L., Rosenthal, Y., Yu, J., 2016. Trace element proxies for surface ocean conditions: a synthesis of culture calibrations with planktic foraminifera. Geochim. Cosmochim. Acta 193, 197–221. https://doi.org/10.1016/j.gca.2016.08.015.

Anand, P., Elderfield, H., Conte, M.H., 2003. Mg/Ca and d18O measurements of planktonic foraminifera from sargasso sea. suppl. anand P Al 2003 calibration MgCa thermom. planktonic foraminifera sediment trap time ser. Paleoceanogr. https://doi.org/10.1594/PANGAEA.740070. 182 1050 Httpsdoiorg1010292002PA000846.

Bahr, A., Schönfeld, J., Hoffmann, J., Voigt, S., Aurahs, R., Kucera, M., Flögel, S., Jentzen, A., Gerdes, A., 2013. Comparison of Ba/Ca and δOWATER18 as freshwater proxies: a multi-species core-top study on planktonic foraminifera from the vicinity of the orinoco river mouth. Earth Planet. Sci. Lett. 383, 45–57. https://doi.org/10.1016/j.epsl.2013.09.036.

Barker, S., Greaves, M., Elderfield, H., 2003. A study of cleaning procedures used for foraminiferal Mg/Ca paleothermometry. Geochem. Geophys. Geosyst. 4. https://doi.

org/10.1029/2003GC000559.
Barras, C., Mouret, A., Nardelli, M.P., Metzger, E., Petersen, J., La, C., Filipsson, H.L., Jorissen, F., 2018. Experimental calibration of manganese incorporation in foraminiferal calcite. Geochim. Cosmochim. Acta 237, 49–64. https://doi.org/10.1016/j.gca.2018.06.009.
Bijma, J., Faber, W.W., Hemleben, C., 1990. Temperature and salinity limits for growth and survival of some planktonic foraminifers in laboratory cultures. J. Foraminifer. Res. 20, 95–116.
Bohaty, S.M., Zachos, J.C., Delaney, M.L., 2012. Foraminiferal Mg/Ca evidence for Southern Ocean cooling across the eocene–oligocene transition. Earth Planet. Sci. Lett. 317–318, 251–261. https://doi.org/10.1016/j.epsl.2011.11.037.
Boyle, E.A., 1983. Manganese carbonate overgrowths on foraminifera tests. Geochim. Cosmochim. Acta 47, 1815–1819. https://doi.org/10.1016/0016-7037(83)90029-7.
Boyle, E.A., 1995. Limits on benthic foraminiferal chemical analyses as precise measures of environmental properties. J. Foraminifer. Res. 10–2113.
Boyle, E.A., Keigwin, L.D., 1985. Comparison of Atlantic and Pacific paleochemical records for the last 215,000 years: changes in deep ocean circulation and chemical inventories. Earth Planet. Sci. Lett. 76, 135–150. https://doi.org/10.1016/0012-821X(85)90154-2.
Branson, O., Redfern, S.A.T., Tyliszczak, T., Sadekov, A., Langer, G., Kimoto, K., Elderfield, H., 2013. The coordination of Mg in foraminiferal calcite. Earth Planet. Sci. Lett. 383, 134–141. https://doi.org/10.1016/j.epsl.2013.09.037.
Casford, J.S.L., Rohling, E.J., Abu-Zied, R.H., Fontanier, C., Jorissen, F.J., Leng, M.J., Schmiedl, G., Thomson, J., 2003. A dynamic concept for eastern mediterranean circulation and oxygenation during sapropel formation. Palaeogeogr. Palaeoclimatol. Palaeoecol. 190, 103–119. https://doi.org/10.1016/S0031-0182(02)00601-6.
Castañeda, I.S., Schefuß, E., Pätzold, J., Sinninghe Damsté, J.S., Weldeab, S., Schouten, S., 2010. Millennial-scale sea surface temperature changes in the eastern Mediterranean (Nile River Delta region) over the last 27,000 years. Paleoceanography 25https://doi.org/10.1029/2009PA001740. PA1208.
Cita, M.B., Vergnaud-Grazzini, C., Robert, C., Chamley, H., Ciaranfi, N., d'Onofrio, S., 1977. Paleoclimatic record of a long deep sea core from the eastern mediterranean. Quat. Res. 8, 205–235. https://doi.org/10.1016/0033-5894(77)90046-1.
de Garidel-Thoron, T., Rosenthal, Y., Bassinot, F., Beaufort, L., 2005. Stable sea surface temperatures in the western Pacific warm pool over the past 1.75 million years. Nature 433, 294–298. https://doi.org/10.1038/nature03189.
De Lange, G.J., Thomson, J., Reitz, A., Slomp, C.P., Speranza Principato, M., Erba, E., Corselli, C., 2008. Synchronous basin-wide formation and redox-controlled preservation of a Mediterranean sapropel. Nat. Geosci. 1, 606–610. https://doi.org/10.1038/ngeo283.
de Nooijer, L.J., Brombacher, A., Mewes, A., Langer, G., Nehrke, G., Bijma, J., Reichart, G.-J., 2017. Ba incorporation in benthic foraminifera. Biogeosciences 14, 3387–3400. https://doi.org/10.5194/bg-14-3387-2017.
deMenocal, P., Ortiz, J., Guilderson, T., Adkins Sarnthein, J., 2000. Abrupt onset and termination of the African Humid Period:: rapid climate responses to gradual insolation forcing. Quat. Sci. Rev. 19, 347–361. https://doi.org/10.1016/S0277-3791(99)00081-5.
De Rijk, S., Jorissen, F.J., Rohling, E.J., Troelstra, S.R., 2000. Organic flux control on bathymetric zonation of Mediterranean benthic foraminifera. Mar. Micropaleontol. 40, 151–166.
Dissard, D., Nehrke, G., Reichart, G.J., Bijma, J., 2010. Impact of seawater pCO2 on calcification and Mg/Ca and Sr/Ca ratios in benthic foraminifera calcite: results from culturing experiments with Ammonia tepida. Biogeosciences 7, 81–93. https://doi.org/10.5194/bg-7-81-2010.
Dueñas-Bohórquez, A., da Rocha, R.E., Kuroyanagi, A., de Nooijer, L.J., Bijma, J., Reichart, G.-J., 2011. Interindividual variability and ontogenetic effects on Mg and Sr incorporation in the planktonic foraminifer Globigerinoides sacculifer. Geochim. Cosmochim. Acta 75, 520–532. https://doi.org/10.1016/j.gca.2010.10.006.
Dueñas-Bohórquez, A., da Rocha, R.E., Kuroyanagi, A., Bijma, J., Reichart, G.-J., 2009. Effect of salinity and seawater calcite saturation state on Mg and Sr incorporation in cultured planktonic foraminifera. Mar. Micropaleontol. 73, 178–189. https://doi.org/10.1016/j.marmicro.2009.09.002.
Dymond, J., Collier, R., 1996. Particulate barium fluxes and their relationships to biological productivity. Deep Sea Res. Part II Top. Stud. Oceanogr. 43, 1283–1308. https://doi.org/10.1016/0967-0645(96)00011-2.
Dymond, J., Suess, E., Lyle, M., 1992. Barium in deep-sea sediment: a geochemical proxy for paleoproductivity. Paleoceanography 7, 163–181. https://doi.org/10.1029/92PA00181.
Eggins, S., De Deckker, P., Marshall, J., 2003. Mg/Ca variation in planktonic foraminifera tests: implications for reconstructing palaeo-seawater temperature and habitat migration. Earth Planet. Sci. Lett. 212, 291–306. https://doi.org/10.1016/S0012-821X(03)00283-8.
Elderfield, H., Vautravers, M., Cooper, M., 2002. The relationship between shell size and Mg/Ca, Sr/Ca, δ18O, and δ13C of species of planktonic foraminifera. Geochem. Geophys. Geosyst. 3, 1–13. https://doi.org/10.1029/2001GC000194.
Elderfield, H., Yu, J., Anand, P., Kiefer, T., Nyland, B., 2006. Calibrations for benthic foraminiferal Mg/Ca paleothermometry and the carbonate ion hypothesis. Earth Planet. Sci. Lett. 250, 633–649. https://doi.org/10.1016/j.epsl.2006.07.041.
Elderfield, H., Greaves, M., Barker, S., Hall, I.R., Tripati, A., Ferretti, P., Crowhurst, S., Booth, L., Daunt, C., 2010. A record of bottom water temperature and seawater δ18O for the Southern Ocean over the past 440kyr based on Mg/Ca of benthic foraminiferal Uvigerina spp. Quat. Sci. Rev. Clim. Last Million Years 29, 160–169. https://doi.org/10.1016/j.quascirev.2009.07.013.
Emeis, K.-C., Struck, U., Schulz, H.-M., Rosenberg, R., Bernasconi, S., Erlenkeuser, H., Sakamoto, T., Martinez-Ruiz, F., 2000. Temperature and salinity variations of Mediterranean Sea surface waters over the last 16,000 years from records of planktonic stable oxygen isotopes and alkenone unsaturation ratios. Palaeogeogr. Palaeoclimatol. Palaeoecol. 158, 259–280. https://doi.org/10.1016/S0031-0182(00)00053-5.
Erez, J., 2003. The source of ions for biomineralization in foraminifera and their implications for paleoceanographic proxies. Rev. Mineral. Geochem. 54, 115–149. https://doi.org/10.2113/0540115.
Ferguson, J.E., Henderson, G.M., Kucera, M., Rickaby, R.E.M., 2008. Systematic change of foraminiferal Mg/Ca ratios across a strong salinity gradient. Earth Planet. Sci. Lett. 265, 153–166. https://doi.org/10.1016/j.epsl.2007.10.011.
Fleitmann, D., Burns, S.J., Mangini, A., Mudelsee, M., Kramers, J., Villa, I., Neff, U., Al-Subbary, A.A., Buettner, A., Hippler, D., Matter, A., 2007. Holocene ITCZ and Indian monsoon dynamics recorded in stalagmites from Oman and Yemen (Socotra). Quat. Sci. Rev. 26, 170–188. https://doi.org/10.1016/j.quascirev.2006.04.012.
Fontanier, C., Mackensen, A., Jorissen, F.J., Anschutz, P., Licari, L., Griveaud, C., 2006. Stable oxygen and carbon isotopes of live benthic foraminifera from the bay of biscay: microhabitat impact and seasonal variability. Mar. Micropaleontol. 58, 159–183. https://doi.org/10.1016/j.marmicro.2005.09.004.
Geerken, E., de Nooijer, L.J., van Dijk, I., Reichart, G.-J., 2018. Impact of salinity on element incorporation in two benthic foraminiferal species with contrasting magnesium contents. Biogeosciences 15, 2205–2218. https://doi.org/10.5194/bg-15-2205-2018.
Glock, N., Eisenhauer, A., Liebetrau, V., Wiedenbeck, M., Hensen, C., Nehrke, G., 2012. EMP and SIMS studies on Mn/Ca and Fe/Ca systematics in benthic foraminifera from the Peruvian OMZ: a contribution to the identification of potential redox proxies and the impact of cleaning protocols. Biogeosciences 9, 341–359. https://doi.org/10.5194/bg-9-341-2012.
Gordon, C.M., Carr, R.A., Larson, R.E., 1970. The influence of environmental factors on the sodium and manganese content of barnacle shells. Limnol. Oceanogr. 15, 461–466.
Grant, K.M., Grimm, R., Mikolajewicz, U., Marino, G., Ziegler, M., Rohling, E.J., 2016. The timing of Mediterranean sapropel deposition relative to insolation, sea-level and African monsoon changes. Quat. Sci. Rev. 140, 125–141. https://doi.org/10.1016/j.quascirev.2016.03.026.
Gray, W.R., Evans, D., 2019. Nonthermal influences on Mg/Ca in planktonic foraminifera: a review of culture studies and application to the last glacial maximum. Paleoceanogr. Paleoclimatol. 34, 306–315. https://doi.org/10.1029/2018PA003517.
Gray, W.R., Weldeab, S., Lea, D.W., Rosenthal, Y., Gruber, N., Donner, B., Fischer, G., 2018. The effects of temperature, salinity, and the carbonate system on Mg/Ca in globigerinoides ruber (white): a global sediment trap calibration. Earth Planet. Sci. Lett. 482, 607–620. https://doi.org/10.1016/j.epsl.2017.11.026.
Grimm, R., Maier-Reimer, E., Mikolajewicz, U., Schmiedl, G., Müller-Navarra, K., Adloff, F., Grant, K.M., Ziegler, M., Lourens, L.J., Emeis, K.-C., 2015. Late glacial initiation of holocene eastern mediterranean sapropel formation. Nat. Commun. 6, 7099. https://doi.org/10.1038/ncomms8099.
Groeneveld, J., Filipsson, H.L., 2013. Mg/Ca and Mn/Ca ratios in benthic foraminifera: the potential to reconstruct past variations in temperature and hypoxia in shelf regions. Biogeosciences 10, 5125–5138. https://doi.org/10.5194/bg-10-5125-2013.
Guay, C.K., Kenison Falkner, K., 1997. Barium as a tracer of arctic halocline and river waters. Deep Sea Res. Part II Top. Stud. Oceanogr. 44, 1543–1569. https://doi.org/10.1016/S0967-0645(97)00066-0.
Guay, C.K., Kenison Falkner, K., 1998. A survey of dissolved barium in the estuaries of major arctic rivers and adjacent seas. Cont. Shelf Res. 18, 859–882. https://doi.org/10.1016/S0278-4343(98)00023-5.
Hamann, Y., Ehrmann, W., Schmiedl, G., Kuhnt, T., 2009. Modern and late quaternary clay mineral distribution in the area of the SE Mediterranean Sea. Quat. Res. 71, 453–464. https://doi.org/10.1016/j.yqres.2009.01.001.
Hammer, O., Harper, D.A.T., Ryan, P.D., 2001. PAST: paleontological statistics software package for education and data analysis. Paleontol. Electron. 4 (1), 1–9.
Hasenfratz, A.P., Martínez-García, A., Jaccard, S.L., Vance, D., Wälle, M., Greaves, M., Haug, G.H., 2017. Determination of the Mg/Mn ratio in foraminiferal coatings: an approach to correct Mg/Ca temperatures for Mn-rich contaminant phases. Earth Planet. Sci. Lett. 457, 335–347. https://doi.org/10.1016/j.epsl.2016.10.004.
Hassoun, A.E.R., Fakhri, M., Raad, N., Abboud-Abi Saab, M., Gemayel, E., De Carlo, E.H., 2019. The carbonate system of the Eastern-most Mediterranean Sea, Levantine Subbasin: variations and drivers. In: Deep Sea Res. Part II Top. Stud. Oceanogr., Revisiting the Eastern Mediterranean: Recent Knowledge on the Physical, Biogeochemical and Ecosystemic States and Trends (Volume I). vol. 164. pp. 54–73. https://doi.org/10.1016/j.dsr2.2019.03.008.
Hennekam, R., de Lange, G., 2012. X-ray fluorescence core scanning of wet marine sediments: methods to improve quality and reproducibility of high-resolution paleoenvironmental records. Limnol. Oceanogr. Methods 10, 991–1003. https://doi.org/10.4319/lom.2012.10.991.
Hennekam, R., Jilbert, T., Schnetger, B., de Lange, G.J., 2014. Solar forcing of Nile discharge and sapropel S1 formation in the early- to Mid-Holocene Eastern Mediterranean. Paleoceanography 2014https://doi.org/10.1002/2013PA002553. PA002553.
Hester, K., Boyle, E., 1982. Water chemistry control of cadmium content in recent benthic foraminifera. Nature 298, 260–262. https://doi.org/10.1038/298260a0.
Hintz, C.J., Shaw, T.J., Bernhard, J.M., Chandler, G.T., McCorkle, D.C., Blanks, J.K., 2006. Trace/minor element:calcium ratios in cultured benthic foraminifera. Part II: ontogenetic variation. Geochim. Cosmochim. Acta 70, 1964–1976. https://doi.org/10.1016/j.gca.2005.12.019.
Hönisch, B., Allen, K.A., Lea, D.W., Spero, H.J., Eggins, S.M., Arbuszewski, J., deMenocal, P., Rosenthal, Y., Russell, A.D., Elderfield, H., 2013. The influence of salinity on Mg/Ca in planktic foraminifers – evidence from cultures, core-top sediments and complementary δ18O. Geochim. Cosmochim. Acta 121, 196–213. https://doi.org/10.

1016/j.gca.2013.07.028.
Honisch, B., Allen, K.A., Lea, D.W., Spero, H.J., Eggins, S.M., Arbuszewski, J., deMenocal, P.B., Rosenthal, Y., Russell, A.D., Elderfield, H., 2013. The influence of salinity on Mg/Ca in planktic foraminifers-evidence from cultures. In: Core-top Sediments and Complementary δ18O.
Hoogakker, B.A.A., Klinkhammer, G.P., Elderfield, H., Rohling, E.J., Hayward, C., 2009. Mg/Ca paleothermometry in high salinity environments. Earth Planet. Sci. Lett. 284, 583–589. https://doi.org/10.1016/j.epsl.2009.05.027.
Jilbert, T., Reichart, G.-J., Mason, P., de Lange, G.J., 2010. Short-time-scale variability in ventilation and export productivity during the formation of Mediterranean sapropel S1. Paleoceanography 25. https://doi.org/10.1029/2010PA001955.
Jochum, K.P., Weis, U., Stoll, B., Kuzmin, D., Yang, Q., Raczek, I., Jacob, D.E., Stracke, A., Birbaum, K., Frick, D.A., Günther, D., Enzweiler, J., 2011. Determination of reference values for NIST SRM 610–617 glasses following ISO guidelines. Geostand. Geoanal. Res. 35, 397–429. https://doi.org/10.1111/j.1751-908X.2011.00120.x.
Kallel, N., Paterne, M., Duplessy, J., Vergnaudgrazzini, C., Pujol, C., Labeyrie, L., Arnold, M., Fontugne, M., Pierre, C., 1997. Enhanced rainfall in the mediterranean region during the last sapropel event. Oceanol. Acta 20, 697–712.
Katz, M.E., Cramer, B.S., Franzese, A., Hönisch, B., Miller, K.G., Rosenthal, Y., Wright, J.D., 2010. Traditional and emerging geochemical proxies in foraminifera. J. Foraminifer. Res. 40, 165–192. https://doi.org/10.2113/gsjfr.40.2.165.
Klinkhammer, G.P., Mix, A.C., Haley, B.A., 2009. Increased dissolved terrestrial input to the coastal ocean during the last deglaciation. Geochem. Geophys. Geosyst. 10. https://doi.org/10.1029/2008GC002219.
Koho, K.A., de Nooijer, L.J., Reichart, G.J., 2015. Combining benthic foraminiferal ecology and shell Mn/Ca to deconvolve past bottom water oxygenation and paleoproductivity. Geochim. Cosmochim. Acta 165, 294–306. https://doi.org/10.1016/j.gca.2015.06.003.
Koho, K.A., de Nooijer, L.J., Fontanier, C., Toyofuku, T., Oguri, K., Kitazato, H., Reichart, G.-J., 2017. Benthic foraminiferal Mn / Ca ratios reflect microhabitat preferences. Biogeosciences 14, 3067–3082. https://doi.org/10.5194/bg-14-3067-2017.
Kontakiotis, G., Mortyn, P.G., Antonarakou, A., Martínez-Botí, M.A., Triantaphyllou, M.V., 2011. Field-based validation of a diagenetic effect on G. ruber Mg/Ca paleothermometry: core top results from the aegean sea (eastern Mediterranean). Geochem. Geophys. Geosyst. 12. https://doi.org/10.1029/2011GC003692.
Kress, N., Gertman, I., Herut, B., 2014. Temporal evolution of physical and chemical characteristics of the water column in the easternmost levantine basin (Eastern Mediterranean Sea) from 2002 to 2010. J. Mar. Syst. 135, 6–13. https://doi.org/10.1016/j.jmarsys.2013.11.016.
Kuhnt, T., Schmiedl, G., Ehrmann, W., Hamann, Y., Hemleben, C., 2007. Deep-sea ecosystem variability of the Aegean Sea during the past 22 kyr as revealed by Benthic Foraminifera. Mar. Micropaleontol. 64, 141–162. https://doi.org/10.1016/j.marmicro.2007.04.003.
Kuhnt, T., Schmiedl, G., Ehrmann, W., Hamann, Y., Andersen, N., 2008. Stable isotopic composition of Holocene benthic foraminifers from the Eastern Mediterranean Sea: past changes in productivity and deep water oxygenation. Palaeogeogr. Palaeoclimatol. Palaeoecol. 268, 106–115. https://doi.org/10.1016/j.palaeo.2008.07.010.
Langer, G., Sadekov, A., Thoms, S., Keul, N., Nehrke, G., Mewes, A., Greaves, M., Misra, S., Reichart, G.-J., de Nooijer, L.J., Bijma, J., Elderfield, H., 2016. Sr partitioning in the benthic foraminifera ammonia aomoriensis and amphistegina lessonii. Chem. Geol. 440, 306–312. https://doi.org/10.1016/j.chemgeo.2016.07.018.
Lea, D.W., 1999. Trace elements in foraminiferal calcite. In: Gupta, B.K. (Ed.), Modern Foraminifera, pp. 259–277 UK.
Lea, D.W., 2014. 8.14-Elemental and isotopic proxies of past ocean temperatures. In: Holland, H.D., Turekian, K.K. (Eds.), Treatise on Geochemistry, 2nd ed. Elsevier, Oxford, pp. 373–397. https://doi.org/10.1016/B978-0-08-095975-7.00614-8.
Lea, D., Boyle, E., 1989. Barium content of benthic foraminifera controlled by bottom-water composition. Nature 338, 751–753. https://doi.org/10.1038/338751a0.
Lea, D.W., Boyle, E.A., 1990. A 210,000-year record of barium variability in the deep Northwest Atlantic Ocean. Nature 347, 269–272. https://doi.org/10.1038/347269a0.
Lea, D.W., Spero, H.J., 1992. Experimental determination of barium uptake in shells of the planktonic foraminifera Orbulina universa at 22°C. Geochim. Cosmochim. Acta 56, 2673–2680. https://doi.org/10.1016/0016-7037(92)90352-J.
Lea, D.W., Mashiotta, T.A., Spero, H.J., 1999. Controls on magnesium and strontium uptake in planktonic foraminifera determined by live culturing. Geochim. Cosmochim. Acta 63, 2369–2379. https://doi.org/10.1016/S0016-7037(99)00197-0.
Lea, D.W., Pak, D.K., Spero, H.J., 2000. climate impact of late quaternary equatorial pacific sea surface temperature variations. Science 289, 1719–1724. https://doi.org/10.1126/science.289.5485.1719.
Lear, C.H., Rosenthal, Y., Slowey, N., 2002. Benthic foraminiferal Mg/Ca-paleothermometry: a revised core-top calibration. Geochim. Cosmochim. Acta 66, 3375–3387. https://doi.org/10.1016/S0016-7037(02)00941-9.
Liguori, B.T.P., Almeida, M.G.D., Rezende, C.E.D., Liguori, B.T.P., Almeida, M.G.D., Rezende, C.E.D., 2016. Barium and its importance as an indicator of (Paleo)productivity. An. Acad. Bras. Ciênc. 88, 2093–2103. https://doi.org/10.1590/0001-3765201620140592.
Lisiecki, Lorraine E., Raymo, Maureen E., 2005. A pliocene-pleistocene stack of 57 globally distributed benthic δ18O records. Paleoceanography 20. https://doi.org/10.1029/2004PA001071.
Lynch-Stieglitz, J., 2003. Tracers of past ocean circulation. In: Holland, H.D., Turekian, K.K. (Eds.), Treatise on Geochemistry. Pergamon, Oxford, pp. 433–451. https://doi.org/10.1016/B0-08-043751-6/06117-X.
Lynch-Stieglitz, J., Adkins, J.F., Curry, W.B., Dokken, T., Hall, I.R., Herguera, J.C., Hirschi, J.J.-M., Ivanova, E.V., Kissel, C., Marchal, O., Marchitto, T.M., McCave, I.N., McManus, J.F., Mulitza, S., Ninnemann, U., Peeters, F., Yu, E.-F., Zahn, R., 2007. Atlantic meridional overturning circulation during the last glacial maximum. Science 316, 66–69. https://doi.org/10.1126/science.1137127.
Manca, B., Burca, M., Giorgetti, A., Coatanoan, C., Garcia, M.-J., Iona, A., 2004. Physical and biochemical averaged vertical profiles in the Mediterranean regions: an important tool to trace the climatology of water masses and to validate incoming data from operational oceanography. J. Mar. Syst. Tracer Methods Geophys. Fluid Dyn. 48, 83–116. https://doi.org/10.1016/j.jmarsys.2003.11.025.
Mangini, A., Schlosser, P., 1986. The formation of Eastern Mediterranean sapropels. Mar. Geol. 72, 115–124. https://doi.org/10.1016/0025-3227(86)90102-7.
Marchitto, T.M., Broecker, W.S., 2006. Deep water mass geometry in the glacial atlantic ocean: a review of constraints from the paleonutrient proxy Cd/Ca. Geochem. Geophys. Geosyst. 7. https://doi.org/10.1029/2006GC001323.
Marullo, S., Santoleri, R., Malanotte-Rizzoli, P., Bergamasco, A., 1999. The sea surface temperature field in the Eastern Mediterranean from advanced very high resolution radiometer (AVHRR) data. J. Mar. Syst. 20, 83–112. https://doi.org/10.1016/S0924-7963(98)00072-4.
McCorkle, D.C., Martin, P.A., Lea, D.W., Klinkhammer, G.P., 1995. Evidence of a dissolution effect on benthic foraminiferal shell chemistry: δ13C, Cd/Ca, Ba/Ca, and Sr/Ca results from the Ontong Java Plateau. Paleoceanography 10, 699–714. https://doi.org/10.1029/95PA01427.
McKay, C.L., Groeneveld, J., Filipsson, H.L., Gallego-Torres, D., Whitehouse, M.J., Toyofuku, T., Romero, O.E., 2015. A comparison of benthic foraminiferal Mn/Ca and sedimentary Mn/Al as proxies of relative bottom-water oxygenation in the low-latitude NE Atlantic upwelling system. Biogeosciences 12, 5415–5428. https://doi.org/10.5194/bg-12-5415-2015.
Mercone, D., Thomson, J., Croudace, I.W., Siani, G., Paterne, M., Troelstra, S., 2000. Duration of S1, the most recent sapropel in the eastern Mediterranean Sea, as indicated by accelerator mass spectrometry radiocarbon and geochemical evidence. Paleoceanography 15, 336–347. https://doi.org/10.1029/1999PA000397.
Mewes, A., Langer, G., Reichart, G.-J., de Nooijer, L.J., Nehrke, G., Bijma, J., 2015. The impact of Mg contents on Sr partitioning in benthic foraminifers. Chem. Geol. 412, 92–98. https://doi.org/10.1016/j.chemgeo.2015.06.026.
Mezger, E.M., Nooijer, L.J., Boer, W., Brummer, G.J.A., Reichart, G.J., 2016. Salinity controls on Na incorporation in Red Sea planktonic foraminifera. Paleoceanography 31, 1562–1582. https://doi.org/10.1002/2016PA003052.
Mezger, E.M., de Nooijer, L.J., Siccha, M., Brummer, G.-J.A., Kucera, M., Reichart, G.-J., 2018. Taphonomic and ontogenetic effects on Na/Ca and Mg/Ca in spinose planktonic foraminifera from the red sea. Geochem. Geophys. Geosyst. 19, 4174–4194. https://doi.org/10.1029/2018GC007852.
Mezger, E.M., Nooijer, L.J., de Bertlich, J., Bijma, J., Nürnberg, D., Reichart, G.-J., 2019. Planktonic foraminiferal spine versus shell carbonate Na incorporation in relation to salinity. Biogeosciences 16, 1147–1165. https://doi.org/10.5194/bg-16-1147-2019.
Millero, F.J., Schreiber, D.R., 1982. Use of the ion pairing model to estimate activity coefficients of the ionic components of natural waters. Am. J. Sci. 282, 1508–1540. https://doi.org/10.2475/ajs.282.9.1508.
Mojtahid, M., Manceau, R., Schiebel, R., Hennekam, R., de Lange, G.J., 2015. Thirteen thousand years of southeastern Mediterranean climate variability inferred from an integrative planktic foraminiferal-based approach. Paleoceanography 30, 402–422. https://doi.org/10.1002/2014PA002705.
Myers, P.G., Haines, K., Rohling, E.J., 1998. Modeling the paleocirculation of the Mediterranean: the last glacial maximum and the holocene with emphasis on the formation of sapropel S1. Paleoceanography 13, 586–606. https://doi.org/10.1029/98PA02736.
Nehrke, G., Keul, N., Langer, G., de Nooijer, L.J., Bijma, J., Meibom, A., 2013. A new model for biomineralization and trace-element signatures of foraminifera tests. Biogeosciences 10, 6759–6767. https://doi.org/10.5194/bg-10-6759-2013.
Ní Fhlaithearta, S., Reichart, G.-J., Jorissen, F.J., Fontanier, C., Rohling, E.J., Thomson, J., De Lange, G.J., 2010. Reconstructing the seafloor environment during sapropel formation using benthic foraminiferal trace metals, stable isotopes, and sediment composition. Paleoceanography 25, PA4225. https://doi.org/10.1029/2009PA001869.
Nolet, G.J., Corliss, B.H., 1990. Benthic foraminiferal evidence for reduced deep-water circulation during sapropel deposition in the eastern Mediterranean. Mar. Geol. 94, 109–130. https://doi.org/10.1016/0025-3227(90)90106-T.
Nürnberg, D., Bijma, J., Hemleben, C., 1996. Assessing the reliability of magnesium in foraminiferal calcite as a proxy for water mass temperatures. Geochim. Cosmochim. Acta 60, 803–814. https://doi.org/10.1016/0016-7037(95)00446-7.
Nürnberg, D., Müller, A., Schneider, R.R., 2000. Paleo-sea surface temperature calculations in the equatorial east Atlantic from Mg/Ca ratios in planktic foraminifera: a comparison to sea surface temperature estimates from U37K′, oxygen isotopes, and foraminiferal transfer function. Paleoceanography 15, 124–134. https://doi.org/10.1029/1999PA000370.
Paytan, A., Griffith, E.M., 2007. Marine barite: recorder of variations in ocean export productivity. In: Deep Sea Res. Part II Top. Stud. Oceanogr., The Role of Marine Organic Carbon and Calcite Fluxes in Driving Global Climate Change, Past and Future. vol. 54. pp. 687–705. https://doi.org/10.1016/j.dsr2.2007.01.007.
Pross, J., Kotthoff, U., Müller, U.C., Peyron, O., Dormoy, I., Schmiedl, G., Kalaitzidis, S., Smith, A.M., 2009. Massive perturbation in terrestrial ecosystems of the Eastern Mediterranean region associated with the 8.2 kyr B.P. climatic event. Geology 37, 887–890. https://doi.org/10.1130/G25739A.1.
Ramsey, C.B., 2009. Bayesian analysis of radiocarbon dates. Radiocarbon 51, 337–360. https://doi.org/10.2458/azu_js_rc.51.3494.
Ravelo, A.C., Hillaire-Marcel, C., 1999. Chapter eighteen the use of oxygen and carbon isotopes of foraminifera in paleoceanography. In: Sen Gupta, Barun K. (Ed.), Modern

Foraminifera, pp. 371 The Netherlands.
Reichart, G.-J., Jorissen, F., Anschutz, P., Mason, P.R.D., 2003. Single foraminiferal test chemistry records the marine environment. Geology 31, 355–358. https://doi.org/10.1130/0091-7613(2003)031<0355:SFTCRT>2.0.CO;2.
Reimer, P.J., Baillie, M.G.L., Bard, E., Bayliss, A., Beck, J.W., Blackwell, P.G., Ramsey, C.B., Buck, C.E., Burr, G.S., Edwards, R.L., others, 2009. IntCal09 and MARINE09 Radiocarbon age Calibration Curves, 0–50,000 years cal BP. vol. 51. pp. 1111–1150.
Revel, M., Ducassou, E., Grousset, F.E., Bernasconi, S.M., Migeon, S., Revillon, S., Mascle, J., Murat, A., Zaragosi, S., Bosch, D., 2010. 100,000 years of african monsoon variability recorded in sediments of the nile margin. Quat. Sci. Rev. 29, 1342–1362. https://doi.org/10.1016/j.quascirev.2010.02.006.
Revel, M., Colin, C., Bernasconi, S., Combourieu-Nebout, N., Ducassou, E., Grousset, F.E., Rolland, Y., Migeon, S., Bosch, D., Brunet, P., Zhao, Y., Mascle, J., 2014. 21,000 Years of Ethiopian African monsoon variability recorded in sediments of the western Nile deep-sea fan. Reg. Environ. Chang. 1–12. https://doi.org/10.1007/s10113-014-0588-x.
Rohling, E.J., 1994. Review and new aspects concerning the formation of eastern mediterranean sapropels. Mar. Geol. 122, 1–28. https://doi.org/10.1016/0025-3227(94)90202-X.
Rohling, E., Cooke, S., 2003. Stable oxygen and carbon isotopes in foraminiferal carbonate shells. In: Mod. Foraminifera, Springer Netherlands Part III, pp. 239–258.
Rohling, E., Mayewski, P., Abu-Zied, R., Casford, J., Hayes, A., 2002. Holocene atmosphere-ocean interactions: records from Greenland and the Aegean Sea. Clim. Dyn. 18, 587–593. https://doi.org/10.1007/s00382-001-0194-8.
Rohling, E.J., Sprovieri, M., Cane, T., Casford, J.S.L., Cooke, S., Bouloubassi, I., Emeis, K.C., Schiebel, R., Rogerson, M., Hayes, A., Jorissen, F.J., Kroon, D., 2004. Reconstructing past planktic foraminiferal habitats using stable isotope data: a case history for Mediterranean sapropel S5. Mar. Micropaleontol. 50, 89–123. https://doi.org/10.1016/S0377-8398(03)00068-9.
Rohling, E.J., Foster, G.L., Grant, K.M., Marino, G., Roberts, A.P., Tamisiea, M.E., Williams, F., 2014. Sea-level and deep-sea-temperature variability over the past 5.3 million years. Nature 508, 477–482. https://doi.org/10.1038/nature13230.
Rohling, E.J., Marino, G., Grant, K.M., 2015. Mediterranean climate and oceanography, and the periodic development of anoxic events (sapropels). Earth-Sci. Rev. 143, 62–97. https://doi.org/10.1016/j.earscirev.2015.01.008.
Rosenthal, Y., Boyle, E.A., Slowey, N., 1997. Temperature control on the incorporation of magnesium, strontium, fluorine, and cadmium into benthic foraminiferal shells from little bahama bank: prospects for thermocline paleoceanography. Geochim. Cosmochim. Acta 61, 3633–3643. https://doi.org/10.1016/S0016-7037(97)00181-6.
Rosenthal, Y., Lear, C.H., Oppo, D.W., Linsley, B.K., 2006. Temperature and carbonate ion effects on Mg/Ca and Sr/Ca ratios in benthic foraminifera: aragonitic species hoeglundina elegans. Paleoceanography 21, PA1007. https://doi.org/10.1029/2005PA001158.
Rosenthal, Y., Morley, A., Barras, C., Katz, M.E., Jorissen, F., Reichart, G.-J., Oppo, D.W., Linsley, B.K., 2011. Temperature calibration of Mg/Ca ratios in the intermediate water benthic foraminifer hyalinea balthica. Geochem. Geophys. Geosyst. 12, Q04003. https://doi.org/10.1029/2010GC003333.
Rossignol-Strick, M., Nesteroff, W., Olive, P., Vergnaud-Grazzini, C., 1982. After the deluge: Mediterranean stagnation and sapropel formation. Nature 295, 105–110. https://doi.org/10.1038/295105a0.
Rucker, J.B., Valentine, J.W., 1961. Salinity response of trace element concentration in crassostrea virginica. Nature 190, 1099–1100. https://doi.org/10.1038/1901099a0.
Russell, A.D., Emerson, S., Nelson, B.K., Erez, J., Lea, D.W., 1994. Uranium in foraminiferal calcite as a recorder of seawater uranium concentrations. Geochim. Cosmochim. Acta 58, 671–681. https://doi.org/10.1016/0016-7037(94)90497-9.
Schmiedl, G., Kuhnt, T., Ehrmann, W., Emeis, K.-C., Hamann, Y., Kotthoff, U., Dulski, P., Pross, J., 2010. Climatic forcing of eastern Mediterranean deep-water formation and benthic ecosystems during the past 22 000 years. Quat. Sci. Rev. 29, 3006–3020. https://doi.org/10.1016/j.quascirev.2010.07.002.
Schmittner, A., Bostock Helen, C., Olivier, Cartapanis, Curry William, B., Filipsson Helena, L., Galbraith Eric, D., Julia, Gottschalk, Carlos, Herguera Juan, Babette, Hoogakker, Jaccard Samuel, L., Lisiecki Lorraine, E., Lund David, C., Gema, Martínez-Méndez, Jean, Lynch-Stieglitz, Andreas, Mackensen, Elisabeth, Michel, Mix Alan, C., Oppo Delia, W., Peterson Carlye, D., Janne, Repschläger, Sikes Elisabeth, L., Spero Howard, J., Claire, Waelbroeck, 2017. Calibration of the carbon isotope composition (δ13C) of benthic foraminifera. Paleoceanography 32, 512–530. https://doi.org/10.1002/2016PA003072.
Schneider, A., Crémière, A., Panieri, G., Lepland, A., Knies, J., 2017. Diagenetic alteration of benthic foraminifera from a methane seep site on Vestnesa Ridge (NW Svalbard). Deep Sea Res. Part Oceanogr. Res. 123, 22–34. https://doi.org/10.1016/j.dsr.2017.03.001.
Segev, E., Erez, J., 2006. Effect of Mg/Ca ratio in seawater on shell composition in shallow benthic foraminifera. Geochem. Geophys. Geosyst. 7. https://doi.org/10.1029/2005GC000969.
Sexton, P.F., Wilson, P.A., Pearson, P.N., 2006. Microstructural and geochemical perspectives on planktic foraminiferal preservation: “Glassy” versus “Frosty.”. Geochem. Geophys. Geosyst. 7. https://doi.org/10.1029/2006GC0012doi:91.
Shackleton, N.J., 1974. Attainment of isotopic equilibrium between ocean water and the benthonic foraminifera genus Uvigerina: isotopic changes in the ocean during the last glacial. In: Colloques Internationaux du C.N.R.S. EPIC3England, pp. 203–209.
Skinner, L.C., Shackleton, N.J., Elderfield, H., 2003. Millennial-scale variability of deep-water temperature and δ18Odw indicating deep-water source variations in the Northeast Atlantic, 0–34 cal ka BP. Geochem. Geophys. Geosyst. 4. https://doi.org/10.1029/2003GC000585.
Statham, P.J., Burton, J.D., 1986. Dissolved manganese in the North Atlantic Ocean, 0–35°N. Earth Planet. Sci. Lett. 79, 55–65. https://doi.org/10.1016/0012-821X(86)90040-3.
Stuiver, M., Braziunas, T.F., 1993. Sun, ocean, climate and atmospheric 14CO2: an evaluation of causal and spectral relationships. Holocene 3, 289–305. https://doi.org/10.1177/095968369300300401.
Stuiver, M., Reimer, P.J., Bard, E., Beck, J.W., Burr, G.S., Hughen, K.A., Kromer, B., McCormac, G., van der Plicht, J., Spurk, M., 1998. INTCAL98 radiocarbon age calibration, 24,000-0 cal BP. Radiocarbon 40, 1041–1083.
Tachikawa, K., Vidal, L., Cornuault, M., Garcia, M., Pothin, A., Sonzogni, C., Bard, E., Menot, G., Revel, M., 2015. Eastern Mediterranean Sea circulation inferred from the conditions of S1 sapropel deposition. Clim. Past 11, 855–867. https://doi.org/10.5194/cp-11-855-2015.
Tierney, J.E., Tingley, M.P., 2018. BAYSPLINE: A New Calibration for the Alkenone Paleothermometer. Paleoceanogr. Paleoclimatology 33, 281–301. https://doi.org/10.1002/2017PA003201.
Thomson, J., Mercone, D., De Lange, G.J., Van Santvoort, P.J.M., 1999. Review of recent advances in the interpretation of eastern Mediterranean sapropel S1 from geochemical evidence. Mar. Geol. 153, 77–89. https://doi.org/10.1016/S0025-3227(98)00089-9.
Toyofuku, T., Kitazato, H., Kawahata, H., Tsuchiya, M., Nohara, M., 2000. Evaluation of Mg/Ca thermometry in foraminifera: comparison of experimental results and measurements in nature. Paleoceanography 15, 456–464. https://doi.org/10.1029/1999PA000460.
Triantaphyllou, M.V., Ziveri, P., Gogou, A., Marino, G., Lykousis, V., Bouloubassi, I., Emeis, K.-C., Kouli, K., Dimiza, M., Rosell-Melé, A., Papanikolaou, M., Katsouras, G., Nunez, N., 2009. Late Glacial–Holocene climate variability at the south-eastern margin of the Aegean Sea. Mar. Geol. 266, 182–197. https://doi.org/10.1016/j.margeo.2009.08.005.
Triantaphyllou, M.V., Gogou, A., Dimiza, M.D., Kostopoulou, S., Parinos, C., Roussakis, G., Geraga, M., Bouloubassi, I., Fleitmann, D., Zervakis, V., Velaoras, D., Diamantopoulou, A., Sampatakaki, A., Lykousis, V., 2016. Holocene climatic optimum centennial-scale paleoceanography in the NE Aegean (Mediterranean Sea). Geo-Mar. Lett. 36, 51–66. https://doi.org/10.1007/s00367-015-0426-2.
UNEP/MAP, 2012. State of the Mediterranean Marine and Coastal Environment.
van der Meer, M.T.J., Baas, M., Rijpstra, W.I.C., Marino, G., Rohling, E.J., Sinninghe Damsté, J.S., Schouten, S., 2007. Hydrogen isotopic compositions of long-chain alkenones record freshwater flooding of the Eastern Mediterranean at the onset of sapropel deposition. Earth Planet. Sci. Lett. 262, 594–600. https://doi.org/10.1016/j.epsl.2007.08.014.
Vergnaud-Grazzini, C., Ryan, W.B.F., Bianca Cita, M., 1977. Stable isotopic fractionation, climate change and episodic stagnation in the Eastern Mediterranean during the late quaternary. Mar. Micropaleontol. 2, 353–370. https://doi.org/10.1016/0377-8398(77)90017-2.
Weldeab, S., Lea, D.W., Schneider, R.R., Andersen, N., 2007. Centennial scale climate instabilities in a wet early Holocene West African monsoon. Geophys. Res. Lett. 34, L24702. https://doi.org/10.1029/2007GL031898.
Weldeab, S., Menke, V., Schmiedl, G., 2014. The pace of East African monsoon evolution during the Holocene. Geophys. Res. Lett. 41https://doi.org/10.1002/2014GL059361. 2014GL059361.
Wit, J.C., Reichart, G.-J., Jung, S.J.A., Kroon, D., 2010. Approaches to unravel seasonality in sea surface temperatures using paired single-specimen foraminiferal δ18O and Mg/Ca analyses. Paleoceanography 25, PA4220. https://doi.org/10.1029/2009PA001857.
Wit, J.C., de Nooijer, L.J., Wolthers, M., Reichart, G.J., 2013. A novel salinity proxy based on Na incorporation into foraminiferal calcite. Biogeosciences 10, 6375–6387. https://doi.org/10.5194/bg-10-6375-2013.
Wüst, G., 1961. On the vertical circulation of the Mediterranean Sea. J. Geophys. Res. 66, 3261–3271. https://doi.org/10.1029/JZ066i010p03261.
Ziegler, M., Tuenter, E., Lourens, L.J., 2010. The precession phase of the boreal summer monsoon as viewed from the Eastern Mediterranean (ODP Site 968). Quat. Sci. Rev. 29, 1481–1490. https://doi.org/10.1016/j.quascirev.2010.03.011.